R&D 9314-AN-01

LOW – VELOCITY SPALL TESTING OF Ti – 6Al – 4V ALLOY AND A NEW SPALL CRITERION BASED ON MESO-SCALE

Final Technical Report

by

Principal Investigator: Prof. Janusz R. Klepaczko

(with participation: P. Chevrier and X. Boidin)

August 2003

United States Army

EUROPEAN RESEARCH OFFICE OF THE U.S. ARMY

London, England

Contract Number N62558-02-M-5857

Contractor:

Laboratory of the Mechanics and Physics of Solids,
Metz University, UMR – CNRS 7554
F – 57045 Metz, France

Approved for Public Release
Distribution Unlimited

REPORT DOCUMENTATION PAGE

Form Approved
OMB No. 0704-0188

1. AGENCY USE ONLY (Leave Blank	2. REPORT DATE	3. REPORT TYPE AND DATES COVERED
	Aug. 2003	Final Technical Report

4. TITLE AND SUBTITLE	5. FUNDING NUMBERS
ow-Velocity Spall Testing of Ti-6Al-4V lloy and New Spall Criterion on Mesoscale	C-N62558-02-M-5857
6. AUTHOR(S) .R. KLEPACZKO	
7. PERFORMING ORGANIZATION NAME(S) AND ADDRESS(ES) aboratory of Physics and Mechanics of Materials le du Saulcy, F-57045 METZ cedex 1, FRANCE	8. PERFORMING ORGANIZATION REPORT NUMBER Final Technical Report ERO - LPMM
9. SPONSORING/MONITORING AGENCY NAME(S) AND ADDRESS(ES) uropean Research Office of the U.S. Army Monitor : Dr. S. Sampath	10. SPONSORING/MONITORING AGENCY REPORT NUMBER
11. SUPPLEMENTARY NOTES	
12a. DISTRIBUTION / AVAILABILITY STATEMENT	12b. DISTRIBUTION CODE

13. ABSTRACT (Maximum 200 words)

During the period of the Contract, June 17/02 till June 17/03, the spall testing of Ti-6Al-4V alloy has been performed. The series of plate impact tests (total 11 tests) at different impact velocities (from 290 m/s to 460 m/s) has been completed and the level of the incipient spall stress as a function of the incident pulse duration is determined. The results demonstrate, as expected, an increase of the failure stress when the pulse duration is shorter. A quantitative analysis was performed to determine constants in a global cumulative spall criterion leading to time-depend failure. The Scanning Electron Microscopy (SEM) observation of the spalled surfaces was performed, mainly to identify the physical mechanism of fracture development. Also, some pictures of the specimen cross sections were taken after spalling to observe the relief of the material separation. The quantitative analysis of the pictures have shown that in the meso-scale separation occurs by micro-cracks in the opening mode combined with Adiabatic Shear Bands (ASB). Discussion of a new meso-modeling based on those observations is introduced. In order to gain a deeper insight on the material behavior during spalling the initial microstructure of the Ti-6Al-4V alloy has been examined by microscopy observation, including chemical treatment of the specimen surfaces. The literature survey on spalling of Ti-6Al-4V alloy is also included in the Report.

14. SUBJECTS ITEMS Spall of Ti-6Al-4V Alloy			15. NUMBER OF PAGES 16. PRICE CODE
17. SECURITY CLASSIFICATION OF REPORT UNCLASSIFIED	18. SECURITY CLASSIFICATION OF THIS PAGE UNCLASSIFIED	19. SECURITY CLASSIFICATION OF ABSTRACT UNCLASSIFIED	20. LIMITATION OF ABSTRACT UL

REPORT DOCUMENTATION PAGE

Form Approved
OMB No. 0704-0188

1. AGENCY USE ONLY *(Leave blank)*	2. REPORT DATE	3. REPORT TYPE AND DATES COVERED
	27 JAN 04	FINAL REPORT AUGUST 2003

4. TITLE AND SUBTITLE
LOW-VELOCITY SPALL TESTING OF Ti-6Al-4V ALLOY AND NEW SPALL CRITERION ON MESOSCALE

5. FUNDING NUMBERS
9314AN01
N62558-02-M-5857

6. AUTHOR(S)
PROFESSOR JANUSZ R. KLEPACZKO

7. PERFORMING ORGANIZATION NAME(S) AND ADDRESS(ES)
LABORATORY OF THE MECHANICS AND PHYSICS OF SOLIDS
METZ UNIVERSITY, UMR - CNRS 7554
F - 57045 METZ, FRANCE

8. PERFORMING ORGANIZATION REPORT NUMBER

9. SPONSORING / MONITORING AGENCY NAME(S) AND ADDRESS(ES)
U.S. ARMY - EUROPEAN RESEARCH OFFICE
EDISON HOUSE
223 OLD MARYLEBONE ROAD
LONDON NW1 5TH
UNITED KINGDOM

10. SPONSORING / MONITORING AGENCY REPORT NUMBER

11. SUPPLEMENTARY NOTES

12a. DISTRIBUTION / AVAILABILITY STATEMENT
APPROVED FOR PUBLIC DISTRIBUTION
DISTRIBUTION UNLIMITED
FINAL REPORT

12b. DISTRIBUTION CODE

13. ABSTRACT *(Maximum 200 words)*

14. SUBJECT TERMS
SPALL, ALLOY

15. NUMBER OF PAGES
41

16. PRICE CODE

17. SECURITY CLASSIFICATION OF REPORT	18. SECURITY CLASSIFICATION OF THIS PAGE	19. SECURITY CLASSIFICATION OF ABSTRACT	20. LIMITATION OF ABSTRACT
UNCLASSIFIED	UNCLASSIFIED	UNCLASSIFIED	

LOW – VELOCITY SPALL TESTING OF Ti - 6Al – 4V ALLOY AND A NEW SPALL CRITERION BASED ON MESO-SCALE

Final Technical Report

by

Principal Investigator: Prof. Janusz R. Klepaczko

(with participation: P. Chevrier and X. Boidin)

August 2003

United States Army

EUROPEAN RESEARCH OFFICE OF THE U.S. ARMY

London, England

Contract Number N62558-02-M-5857

Contractor:

Laboratory of the Mechanics and Physics of Solids,

Metz University, UMR – CNRS 7554

F - 57045 Metz, France

EXTENDED ABSTRACT

The main purpose of this research was to examine physical mechanisms of spall fracture for Ti-6Al-4V alloy on the incipient level and to identify the main stages of spalling in the meso-scale. A plate-impact experiment and microscopy observations (SEM and optical) were applied to study material separation in the meso-level, that is from ~5.0 μm to ~100 μm.

In plate impact experiments the lowest impact velocity was searched as a function of the pulse duration in order to determine when the incipient spall occurs. Application of the acoustic approximation permitted determination of the critical normal stress for different pulse duration. Since the minimum stress of spalling is searched for, the acoustic approximation yields a good approximation of the critical failure stress. This is due the fact that plastic deformation (if exists) during passage of the incident compression wave is negligible.

During the contract period the spall testing of Ti-6Al-4V has been completed. The series of tests (total 11 tests) at different impact velocities (from 290 m/s to 460 m/s) have been performed and the level of the normal stress σ_F for the incipient spall as a function of the incident pulse duration t_C has been determined. Such analysis has yielded the preliminary data in the form of the critical tensile stress versus the pulse duration, $\sigma_F(t_C)$. The Scanning Electron Microscopy (SEM) observation of the spalled surfaces was performed showing micro-dimples. Optical microscopy observation of the specimen cross-sections demonstrated presence on the meso-scale a combination of micro-cracks and adiabatic shearing. Those observations are very helpful to identify the physical mechanism of fracture development. The relief of the material separation leads to a new failure criterion on the meso-scale [1,2]. The quantitative statistical analysis of the pictures needs more time and is in progress. A new model of spalling based on two meso-mechanisms of material separation has recently been developed and verified for martensitic armor steel and hard aluminum alloy, [1,2], it confirms all findings by experiment.

In order to gain more deep insight on the material behavior during spalling the initial microstructure of the Ti-6Al-4V alloy has been examined by microscopy observation, including chemical treatment of the surfaces. The literature survey on high strain rate behavior and spalling of Ti-6Al-4V alloy is included in this Report.

Keywords:

Spall fracture, Ti-6Al-4V alloy, Spall criteria, SEM observations.

PRELIMINARY REMARKS

Experimental, microscopy and analytic studies on the effects of different, relatively low, impact velocities involving the planar mode of loading and spalling in titanium alloy is completed. Since titanium alloys are highly rate-sensitive and they exhibit relatively low rate of strain hardening, it was demonstrated for Ti-6Al-4V that spalling under plane wave loading leads to specific mode of failure in the meso-scale that is penny-shaped micro-cracks and almost instantaneous formation of Adiabatic Shear Bands (ASB). As the first step the study of the differences in the critical tensile stress σ_F determined in the global scale as a function of the loading time t_C has been completed. Those differences occur during formation of penny-shaped micro-cracks and localization of the ASB's in hard titanium alloys when the pulse duration change. By performing a series of the plate impact tests with different low velocities and different target thickness it is possible to find *the lowest* tensile stress leading to spalling, an important practical problem. A new, recently proposed, spall criterion based on the dynamics of penny-shaped cracks and the meso-scale ASB's is verified for Ti-6Al-4V, [1,2].

HISTORICAL BACKGROUND

Low-velocity impact techniques are used to study dynamic deformation and failure modes of materials. Typical examples are: so called Taylor test, [3.4], (short rod on rigid plate impact), symmetric impact of two rods, direct impact on Modified Double Shear specimen, [5], (MDS technique) and plate on plate impact, for example [6]. The plate impact experiments are performed in two configurations, that is the normal and oblique impact [6,7]. It is well known for relatively long time that observation of plane waves in materials provides many important data on their dynamic response and failure. A fundamental arrangement of the normal plate impact experiment is the flyer plate and the target plate. The flyer plate is fired from the single stage gas gun at predetermined velocity against stationary target plate. In typical configuration the thickness of the flier is half of the target thickness. This condition assures that the spalling will occur near the mid thickness of the target. Typical diameter of both flier and target may vary from about 50 mm to 100 mm and even larger. In order to eliminate the air cushioning the experiment is performed in vacuum.

In order to trigger spalling in relatively hard metals and alloys the minimum impact velocity should be above 100 m/s. Typical velocity range for one-stage gas guns is from 10 m/s to 1000 m/s. The Laboratory of Physics and Mechanics of Materials (LPMM) of Metz University is equipped with the plate impact facility. Details of that equipment are given in further part of this Report.

Mechanical tests at high strain rates as well as ballistic tests performed on pure titanium and titanium alloys, show its extreme sensitivity to formation of the ASB's, [8 -11]. Consequently, it was recently found that ASB's are also present close to the separation zone in spalled titanium. Studies of spalling combined with fracture dynamics and adiabatic shear banding are the most important part of research for improvement of titanium performance against impact.

The adiabatic shear banding in metals have already been studied for some time, for example [8,9-12] including experiment, analytic solutions and numerical calculations. Recent studies on adiabatic shear banding performed in LPMM-Metz for Ti-6Al-4V, (supported by the U.S. Army Research Laboratory (AMSRL-WM-TA) via the European Research Office of the U.S. Army), yielded data on specific critical conditions when and where the ASBs are formed, [2,13]. Moreover, a systematic study was performed on the failure criterion in adiabatic shearing. It has

appeared that the critical plastic shear strain at failure for Ti-6Al-4V is substantially larger than for VAR 4340 steel with hardness level about 50 HRC, [8,9,14,15]. This finding to some extent supports the result why this Ti alloy is resistant to perforation at high impact velocities [16-19]. Although a number of ASB's are triggered rapidly they stay non-separated for relatively long time. Such behavior is in opposite to VAR 4340 steel or another armor steels.

The open literature on the effect of the nominal velocities of shearing, or impact velocities, indicates that the places where the critical conditions for the onset and evolution of catastrophic thermoplastic shear are reached, with or without phase transformation, act as the sites of fracture initiation in Mode II, [20,21]. This is the case partly observed in spalling in armor steels, [2]. This new observation, combination of Griffith cracks and adiabatic shear bands, constitutes a base for further studies of spalling in the meso-level for hard Ti alloys.

The already proposed global failure criterion for spalling based on the Markov statistics and thermal activation analysis [22] has given very good results when applied to numerical calculations of spalling in hard aluminum alloys [23]. The criterion, discussed later in this Report, has proven its usefulness in numerical calculations of spall in armor steels in GIAT industry.

On the other hand the US Army Research Laboratory (ARL) has recently analyzed the ballistic performance of Ti-6Al-4V titanium alloy against modern penetrators of different aspect ratios (L/D) and compared the results with rolled homogeneous armor (RHA) steel, [16-19]. The unique properties of titanium alloys, i.e. low density, uniform hardness and high strength over the thickness range have demonstrated ballistic performance improvements of up to 60% on a mass basis at ordnance velocities as compared to reference RHA. While titanium alloys had been known to provide increased protection against small arms, the protection provided against modern higher aspect ratio penetrators was impressive. Currently, a major research effort is to develop low cost ballistic titanium alloys. This cost reduction can be achieved by reducing the existing specifications on oxygen content, primarily by increasing the scrap content in the initial Ti-6Al-4V ingots. The ARL has ballistically tested Ti-6Al-4V alloys with oxygen contents as high as 0.30%. Since Mil-Spec Ti-6Al-4V and RHA have similar and overlapping mechanical properties, the ballistic performance results, in part, from strength /density of titanium. However, the mechanical properties RHA vary as a function of plate thickness due to differences in thermo-mechanical processing, e.g., a 38 mm RHA plate has higher strength and hardness than a 152-mm plate. While titanium has poor hardenability in thick sections and cannot be rapidly quenched, excellent mechanical properties can be developed in plates through thermo-mechanical working, for example rolling. Titanium mechanical properties are very uniform through the plate thickness that increases the relative ballistic performance when compared to equivalent thickness of RHA. In thick sections this titanium alloy has significantly better mechanical properties for ballistic application than RHA.

The combination study of adiabatic shearing and spalling of titanium alloys is of major interest to ARL. These combined mechanisms of fast localization of plastic deformation and fracture reduce the overall performance of titanium in a perforation mode where spalling is prevalent which is directly related to adiabatic shear effects. Understanding of the basic shear and spall properties at high rates are absolutely required for use of this material in armored systems. The penetrator / target interaction mechanism in titanium alloys are not, however, well understood. Extensive adiabatic shear banding is evident in the titanium penetration cavities. The poor heat conductivity of titanium alloys along with a low rate of strain hardening induces these localized shear failures through thermal softening which overcome the work-hardening and strain-rate

effects [8-10, 13, 16-18]. In addition, adiabatic shearing in the meso-scale is present, as it is shown in further parts of this Report, in the process of spalling at low impact velocities.

TECHNICAL OBJECTIVES

The main purpose of this study was to clarify, using plate impact experiments and optical methods, the role of short-time local plastic fields occurring in the meso-scale during spalling, including thermal coupling and the local high strain rates. The evolution of spall failure can be taken into account by a criterion based on physical hypotheses. Finally, the shear characteristics of the same titanium alloy obtained earlier within a wide range of strain rates, [8,13], (range of shear strain rate from 10^{-3} 1/s to 10^{5} 1/s) with the Modified Double Shear (MDS) specimen geometry, [5,24-26], can be included into the new failure criterion to predict the global failure stress $\sigma_F(t_C)$ for the plate impact results.

Comparison of the global failure criterion for spalling based on Markov statistics and thermal activation analysis [22] with the new criterion based on the meso-level approach can provide further crucial information how to construct advanced failure criteria for spalling. Such study could advance the state of the art in this area. A relation is sought in respect to titanium properties, that is strain rate and temperature sensitivity, imposed conditions in the form of different loading rates (impact velocities) and experimentally determined global stress level of spalling $\sigma_F(t_C)$. A correlation could be established between susceptibility to catastrophic thermoplastic shear in the meso-scale and material properties including the role of defects that initiate the penny-shaped cracks. This part of the study is be possible by use of the scanning microscopy and non-contact apparatus for roughness measurements of the spalled surfaces. Comparison of constants in the global failure criterion is performed between behavior of VAR 4340 steel, MARS armor steel, and titanium alloy Ti-6Al-4V.

It is hoped that the final results in the form of the meso-scale fractography and new failure criteria, global one and one on the meso-scale, could be used in a more precise evaluation and prediction of spalling. The unique aspects of the proposed study are combination of experimental results, thermo-visco-plastic properties of the alloy studied, formation of ASB, and dynamic fracture on the meso-scale.

It is assumed that this research will have a practical significance in application to more precise design of structures against direct impact.

TECHNICAL APPROACH

The low-velocity plate impact experiments have been carried out at LPMM-Metz since late eighties. A single-stage gas gun is capable firing of projectiles with different shapes and weights at velocity range from 50 m/s to approx. 600 m/s. The LPMM gas gun has four interconnected parts: the pressure chamber of maximum pressure 250 bars with pneumatic breech, the gun barrel 67 mm, the target chamber with optical and electrical windows and the catcher tank with a soft recovery of fliers. The pressure source may be nitrogen, helium or air. All plate impact experiments are performed in vacuum. Part of the gas gun, that is the setup for measurement of impact velocity, target and catcher are shown schematically in Fig.1.

The impact velocity is measured by two sets of light sources, optic fibers, two sets of photodiodes with amplifiers and two time counters. The firing procedure is completely automated and controlled by several gages, including the levels of pressure and vacuum, automaton and two computers. In order to generate plane waves, in both the flyer plate and the target plate, all theirs faces must be flat. It was accomplished via grinding and polishing of all plates.

One of the objectives was to find experimentally the stress level at which the incipient spall occurs at different time of loading. The final result that can be obtained is in the form of $\sigma_F(t_c)$, where σ_F is the global tensile stress for the incipient spall, t_c is the critical time varying in present case from ~3.0 μs to 0.9 μs , [Etch]. Expected result is shown schematically in Fig.2. For relatively long loading pulses the threshold stress σ_{F0} is reached. Below the threshold stress no incipient spall is observed even for very long loading times, typically for hard alloys ~5.0 μs. At shorter loading times the critical stress increases due to rate effects related to visco-plasticity and micro-inertia in the meso-scale.

Ti-6Al-4V ALLOY

One of the most utilized titanium alloys is Ti-6Al-4V, Grade 5 alloy. This α-β alloy has many industrial applications. It is well known that Titanium and its alloys are very sensitive how they are obtained. The technology of fabrication may introduce substantial changes in mechanical behavior. Microstructure of Ti alloys is affected by many technological factors like thermal treatment and cooling rate after rolling. Thus, the production technology is decisive for an optimization of resistance to failure. Since the raw specimens in the form of disks DIA 57.0 mm and of different thickness have been provided by the Army Research Laboratory, Aberdeen, MD, the process of fabrication will not be given here.

The first stage was to verify microstructure of the alloy. After polishing the surfaces were chemically treated and next observed by an optical microscope, [27]. The following stages were applied:

1 – Mechanical polishing with ground paper SiC with grains 2400 avoiding excessive normal force to avoid twinning.

2 - Polishing with diamond paste on nylon fabric with grains 9, 6 and 3 μm up to shiny surface.

3 - Chemical polishing with solution OP-S of Struers containing 30% of oxygen water (H_2O_2).

4 - Chemical treatment of surface with two following solutions:

a – Composition # 1

HF : 4 ml, HNO_3 : 8 ml, H_2O : 500 ml.

b – Composition # 2

HF : 2 ml, HNO_3 : 4 ml, H_2O : 94 ml.

Both solutions yielded good results for Ti-6Al-4V alloy with different time of submersion. In the case of composition #1: 3 min and for composition #2 : 30 and 40 seconds.

The microscopy observation was performed for two directions, that is in the direction of rolling and perpendicular direction. The microstructure in the direction of rolling is shown in Fig.3. The first conclusion is that the microstructure is composed with colonies of grains with different orientations (Widmanstatten microstructure), or typical α+β microstructure. The microstructure in transverse direction is shown in Fig.4. Again, the microstructure is similar, but the grains are smaller. It may be mentioned that the phase α is HCP and β is BCC.

PLATE IMPACT EXPERIMENTS

The gas launcher of LPMM is completely automated. The maximum pressure in the main chamber of volume 1.3×10^4 cm^3 is $p_{max} = 250$ bar, tube diameter D = 57.0 mm and tube length 2.88 m. With nitrogen used in the experiments and the standard mass of striker ~200 g the maximum impact velocity can reach ~600 m/s.

The impact velocity is measured by a setup shown in Fig.1. Three laser diodes emit narrow beams of light which are cut by a flyer. The light cutting is detected by photodiodes placed in front of fiber optic leads. The photodiode signals are amplified and finally are the intervals of light cutting are recorded by two time counters. Application of three light beams enables for exact measurement of the impact velocity at the point of target surface. Since all distances are known, that is between first and second photodiode ΔX_{12} and between second and third ΔX_{23}, also the distance between third photodiode and target, the acceleration / deceleration of flyer can be found and the impact velocity determined exactly.

The specimen grinding and polishing was arranged by LPMM - Metz and the material (titanium alloy) has been be delivered by ARO in the form of machined disks.

A series of eleven good normal impact tests has been performed at room temperature on titanium alloy Ti-6Al-4V within relatively wide range of impact velocities, from 290 m/s to 460 m/s. In order to apply the acoustic approximation different thickness of specimens was applied. The consecutive experiments were performed in such a way that for each impact velocity only one combination of flyer versus target plate thickness was used. Seven combination of the thickness is assumed. For every combination the impact velocity was increased and the level of spalling was examined by perpendicular cutting of the targets. Next, a detailed microscopic evaluation of the targets was performed. The main purpose was to characterize behavior of failure by the stress level of spalling. The specimen dimensions are given in Table 1. Table 2 shows experimental results in the form of loading time, impact velocity and normal stress. Application of the acoustic approximation leads to the following relations:
The time of loading

$$t_c = \frac{2L_i}{C_1} \qquad \text{where} \qquad C_1 = \left(\frac{\lambda + 2\mu}{\rho}\right)^{1/2} \tag{1}$$

where t_c is the loading time, L_i is the current thickness of the target, C_1 is the elastic wave speed of plane waves, λ and μ are Lamé constants (μ is the shear modulus). It is sometimes more convenient to express the wave speeds in terms of Young's E and Poisson's ratio ν, then the speed of plane waves is given by

$$C_1 = \left(\frac{E(1-\nu)}{\rho(1+\nu)(1-2\nu)}\right)^{1/2} \tag{2}$$

When the impact velocity V_0 is exactly measured the stress amplitude of the normal incident wave is given by

$$\sigma=\rho C_1\frac{V_0}{2} \qquad \text{where} \quad v=\frac{V_0}{2} \quad \text{is the mass velocity} \tag{3}$$

This simple approach based on theory of elastic wave propagation is called the "acoustic approximation" and can be only applied for impact velocities close to the Hugoniot elastic limit σ_{YH} given by

$$\sigma_{YH}=\left(1+\frac{2\mu}{\lambda}\right)\sigma_Y \qquad \text{or} \qquad \sigma_{YH}=\frac{1-\nu}{1-2\nu}\sigma_Y \tag{4}$$

where ν it the Poisson's ratio and σ_Y is the elastic limit in one-dimensional stress, obtained by a simple tension test.

The final results are shown in Fig.5 as the spall stress σ_F versus the critical time t_C. During calculation of the critical stress Eq (3) was applied with the elastic wave speed of plane waves as $C_1 = 6.01$ mm/μs. Fig. 5 shows, as expected, that a shorter pulse duration leads to a higher spall stress. For relatively long time of loading of the order $t_C \approx 3.0$ μs the stress of the incipient spall is approximately $\sigma_F \approx 4.25$ GPa. When the pulse duration is $t_C \approx 1.0$ μs the stress of the incipient spall reaches $\sigma \approx 5.75$ GPa. The solid line in Fig.5 is an approximation by a cumulative failure criterion discussed in further part of this Report.

METALLOGRAPHIC EXAMINATION

Matallographic examinations were carried out with optical and Scanning Electron Microscopy (SEM). The initial microstructure was observed via optical microscopy, Figs 3 and 4 and analysis of fractured surfaces was performed with SEM. A fragment of polished cross section of a specimen after complete spalling is shown in Fig.7, impact velocity $V_0 = 370$ m/s and pulse duration $t_C = 1.9$ μs. The picture is similar as to those obtained earlier for hard alloys, for example armor steels. That is formation of a kind of penny-shaped cracks in direction parallel to plane wave and a set of adiabatic shear bands formed perpendicularly to the plane wave (direction of plane wave propagation). A preliminary estimation of the typical dimensions of the penny-shape sizes denoted ΔX_i and the vertical dimensions of adiabatic shearing denoted ΔY_i, leads to the following ranges: $1000\ \mu m < \Delta X_i < 20\ \mu m$ and $40\ \mu m < \Delta Y_i < 15\ \mu m$. Of course, those values are approximate. A complete statistical analysis, similar to that completed for an armor steel [11, 28], will be performed in the future.

Details how the failure occurs are shown in Figs 7 and 8. In Fig.7 the initial stage is clearly visible, material separation by penny-shaped cracks and adiabatic shearing. In Fig.8 a complete separation is clearly visible with the penny-shape crack, $\Delta X \approx 300\ \mu m$, and ASB dimension $\Delta Y_1 \approx 350\ \mu m$ (larger) and $\Delta Y_2 \approx 110\ \mu m$ (smaller).

Since formation of penny-shaped micro-cracks and adiabatic localization in the meso-scale plays a decisive role in spalling, the physically based failure criteria developed during last years, [2,22,23,28], are analyzed for the titanium alloy Ti-6Al-4V in the next parts of this Report. The first one to be discussed represents the global approach and relates the tensile critical stress σ_F with the critical time t_c, thus a direct comparison could be performed with experimental data and

the physical parameters that enter into each criterion could be identified. A more detailed study of the criterion for two materials: aluminum alloy 7020-T6 (Al-Zn-Mg) and armor steel Mars 190 has been published in [2].

THE GLOBAL SPALL CRITERION

It is known that spall fracture depends on numerous factors like loading time, local stress, initial temperature and microstructure. Several formulas exist to predict spall fracture [29]. Those formulations represent three different approaches, namely physical, micro-statistical and purely phenomenological. The departure point is to apply a simple criterion with the lowest number of constants but with some physical meaning. It is generally accepted that the rate and temperature effects are closely related to the thermally activated micro-mechanical processes of fracturing, see review [30]. The temperature-time dependence of strength in solids can be based the kinetic concept of strength, for example [32], which regards fracture as a thermally activated process.

The physical sense of the kinetic equation is defined by the three parameters: the frequency factor, the activation energy and the threshold stress. The activation energy can be interpreted as the magnitude of the energy barrier related to the probability of breaking the bonds defining strength. This constant may be interpreted as a coefficient taking into account the overstress on a bond as compared to the average stress in a solid. A corrected form of failure criterion based on thermal activation must include an overstress $\Delta\sigma_F$ instead of σ_F, this assures a finite value of the threshold stress σ_{F0} at $\Delta\sigma_F = 0$.

Klepaczko [22] has proposed a specific approach to the Boltzmann statistics and has formulated a fracture criterion for short and very short loading times or relatively low homologous temperatures. The critical time to fracture with the threshold stress is given by the relation

$$t_c = t_{c_0} \exp\left(-\frac{\Delta G(\sigma_F)}{kT}\right) \tag{5}$$

where $\Delta G(\sigma_F)$ is the stress dependent free energy of activation taken in the form after Yokobori [33]

$$\Delta G(\sigma_F) = \Delta G_0 \ln\left(\frac{\sigma_F}{\sigma_{F_0}}\right) \tag{6}$$

where t_{c_0} and σ_{F_0} defines the characteristic point for the longest critical time, σ_F is the spall stress. Thus, the following cumulative failure criterion in general form of the following integral has been derived.

$$t_{c_0} = \int_0^{t_c} \left(\frac{\sigma_F(t)}{\sigma_{F_0}}\right)^{\alpha(T)} dt \qquad t_c \le t_{c_0} \quad \text{and} \quad \sigma_F \ge \sigma_{F_0} \tag{7}$$

with

$$\alpha(T) = \Delta G_0/kT \qquad (8)$$

σ_{F_0}, t_{c_0} and $\alpha(T)$ are three material constants at constant temperature. When the process is non-isothermal, as happens locally in the case of spalling, the exponent $\alpha(T)$ is time dependent via changes of temperature during loading or unloading, then $\alpha(T,t)$. The criterion has been generalized for case of a wide variation of the initial temperature by introduction a temperature-dependent threshold stress $\sigma_{F0}(T)$. It is assumed that the threshold stress σ_{F0} decreases with the absolute temperature T in proportion to the temperature dependence of the elastic constants

$$\sigma_{F0}(T)=\hat{\sigma}_{F0}\frac{E(T)}{E_0} \qquad (9)$$

where E_0 is the Young's modulus at $T = 0$, $\hat{\sigma}_{F0}$ is the threshold stress at $T = 0$. Variations of the Young's modulus with temperature is given in [Balk] as

$$\frac{E(T)}{E_0}=\left(1-\frac{T}{T_m}\exp\left(\hat{\theta}\left(1-\frac{T_m}{T}\right)\right)\right) \qquad (10)$$

where T_m is the melting point and $\hat{\theta}$ is the characteristic homologous temperature.

Since this spall criterion is global one, it includes both the brittle micro-mechanisms of separation and dynamic plasticity. Those two factors are superimposed in different proportions signaled by the value of α. Its universality lies in the fact that it has a cumulative character and the exponent α is temperature dependent. When temperature is increased more ductile micro-mechanisms are activated and σ_F increases up to a high level due to enhanced ductility. At homologous temperatures, probably higher then 0.3 to 0.4, another criterion based on dynamic plasticity should be derived. In particular case of square pulse, corresponding to experiments with a square incident compressive wave and with amplitude which is closed to the Hugoniot Elastic Limit (HEL), that is acoustic approximation, the criterion takes the form (Formally, eq.(9) should be integrated with $\sigma_F(t) = \sigma_F H(t)$, where H(t) is the Heaviside step function) :

$$\sigma_F = \sigma_{F_0}\left(\frac{t_{c_0}}{t_c}\right)^{1/\alpha(T)} \qquad t_C < t_{C0} \qquad (11)$$

This criterion is adapted to relatively low and medium temperatures when the kinetics of spalling is triggered by the tensile stress exceeding the threshold stress σ_{F0}. When Eq.(10) is analyzed and plotted in the form $\sigma_F(T)$ for t_c = const, it is found that spall strength slightly increases with temperature. An increase of the failure stress with temperature indicates for an increased contribution of ductile separation. When Eq.(10) is plotted in the form $\sigma_F(t_C)$ for T = const, it is found, as discussed previously and shown in Figs 2 and 5, that the failure stress increases with decreasing of the incident pulse or the critical time t_C.

Assuming the acoustic approximation and rectangular shape of the incident wave, three material constants of the spall criterion in the form of eq.(10) have been found for Ti-6Al-4V

alloy. In order to determine three material constants σ_{F0} , t_{C0} and α all experimental points were analyzed by an optimization procedure and the following were found for Ti-6Al-4V :

$$\sigma_{F0} = 3.85 \text{ GPa} , t_{C0} = 4.0 \ \mu s , \alpha = 3.68$$

Because value of α is directly related to the activation energy ΔG_0 it is possible to calculate value of the energy with Boltzmann constant $k = 6.617*10^{-5}$ eV/K, the result is

$$\Delta G_0 = 0.095 \text{ eV}$$

This is quite reasonable value because the activation energy in thermally activated processes of plastic deformation is usually estimated as $\Delta_{G0}^{pl} = 0.68$ eV , [34], thus this value is much higher than value found via spalling. The ratio of those energies is 0.14 indicating existence in parallel of brittle mechanism of material separation. If the activation energy of spalling were zero then failure would be purely brittle.

It is interesting to note that analysis of experimental data for spalling of aluminum alloy 7020-T6 and armor steel Mars 190 yielded the following set of constants, Al alloy : $\sigma_{F0} = 1.068$ GPa, $\alpha = 1.360$, Mars 190: $\sigma_{F0} = 4.9$ GPa, $\alpha = 2.369$. The activation energies ΔG_0 for these two materials are ΔG_0 (7020-T6) = 0.034eV and ΔG_0 (Mars 190) = 0.059eV. Once again, the values of the mean activation energies for the process of spalling are the global values for all processes involved in the material separation. This is why the activation energy for spalling is always lower than for a « pure » (one-dimensional stress) plasticity. The lowest activation energies to create a free surface by spalling with a small contribution of plasticity, are observed for the almost brittle mechanisms of separation. In conclusion, an assistance of thermal energy of atoms is omnipresent in all mechanisms of fracture and it must be taken into consideration in the time-sensitive threshold stress for spalling. This idea is not quite new, see for example review in [30], but still is a source of new applications.

THE MESO-MODEL OF SPALLING WITH THERMAL COUPLING

In general, the cumulative criteria of spalling, for example that discussed in the previous part of this Report, provide relatively good results in the macro-scale and they are quite useful in numerical codes, for example numerical study in [23] . It appears that in the case of hard metallic alloys the spall involves the mechanism of micro-crack nucleation and propagation and next coalescence of those micro-cracks by adiabatic shearing, see Fig.6. Such approach to analyze spalling is based on mesoscale observations all along the entire cross section of a targets, which quantify the contribution of quasi-brittle and ductile fracture which may also include Adiabatic Shear Banding (ASB). The scenario of failure observed by the Scanning Electron Microscopy (SEM) in Ti-6Al-4V alloy which occurs during spall fracture is in complete agreement with known physical micro-mechanisms. like micro-void formation, [35,36], and Adiabatic Shear Bands (ASB), for example [37,38,12]. The sequence of the micro-mechanisms involved is in agreement with three recognized levels of spalling, that is incipient, intermediate and complete.

Some further observations and conclusions concerning the influence of microstructure on spall kinetics are given below. In general, fracture in metals is a result of combination of two modes of material separation, that is brittle and ductile. The contribution of each mode to the final separation changes with initial test temperature, time of loading, and of course, the initial microstructure. Brittle fracture dominates when a micro-crack is initiated on the mesoscale (0.1 – 10μm) with contribution of a small plastic deformation. Ductile fracture dominates when it

occurs simultaneously with the local plastic deformation larger than a certain threshold. Typical contribution of plasticity in the early stage of failure is the mechanism of micro-voids. For low temperatures and high loading rates including spalling, nucleation is governed by a critical stress, and micro-cracks or micro-voids nucleate and grow from preexisting inhomogeneities like grain boundaries, boundaries of different phases and inclusions. Such initial stage of failure for Ti-6Al-4V alloy tested in RT is shown in Fig.9 after [36]. A significant amount of micro-voids in the region of the expected spall plane was observed. The micro-voids were preferentially located at the boundaries of α grains and lamellar α-β boundaries. It was also observed that the voids were located at triple points as is shown in the lower part of Fig.9. The nucleation on micro-voids is typical for two-phase alloys. The main reason is existence of internal stresses which develop between phases to maintain plastic strain compatibility. It is assumed that under a given state of stress (uniaxial tension) micro-void nucleation is controlled by a certain level of the normal stress threshold. When this stress threshold is exceeded the separation occurs by coalescence of larger voids and local plastic instabilities in the form of ASB. The incipient level of damage can be defined as a limit of those two stages.

The specimen Ti 6(2) 03 has been analyzed by SEM in details, $V_0 = 290$ m/s, $t_C = 3.3$ μs , $\sigma_F = 3.68$ GPa , [27]. It was found that the mechanism of failure is similar to that reported in [35,36]. However, two micro-mechanisms of the initial stages of failure is found. The first one is shown in Fig.10. This is the case when lamellas are oriented in parallel to the plane of impact, then the micro-voids occur at the interface of α-β phases. The second case is shown in Fig.11, in that case the lamellas are inclined to the impact plane, and micro-voids are localized in between junction of two phases. A more advanced stage of such micro-damage is shown in Fig.12 where coalescence of micro-voids is complete. The final material separation is shown in Fig.6. The relief shown in this figure is one of many possibilities and it perhaps depends on the initial hardness of a alloy. It may be mentioned that also other relieves are reported for Ti-6Al-4V in the literature, [36], [39]. This an open problem to be explored. Another unknown factor, very important in the final outcome, is the impact velocity V_0 .

The observations by SEM confirm that the spall process is a result of nucleation, growth and coalescence of micro-cracks when brittle fracture dominates and micro-voids when ductile fracture is more likely. Thus, during the latest stages the spalling is controlled by the local plastic deformation via coalescence of micro-voids and development of local instabilities between them (internal adiabatic shearing or necking of adjacent micro-cavities). It is clear, the microstructure has a direct influence on the mechanism of nucleation, growth and coalescence of micro-cavities or micro-cracks by means of the distribution of nucleation sites and next a high-speed lateral expansion leading to adiabatic plastic bridges.

REMARKS ON STATISTICAL DISTRIBUTION OF DIMPLES

This part of the Report is addresses possibility of detailed microscopic measurements of the spall surfaces in order to determine of statistical distribution of horizontal micro-segments of fracture surface of targets, corresponding to expansion and coalescence of micro-cavities in horizontal direction (parallel to plane wave), and vertical segments, corresponding to ductile fracture and /or adiabatic shear banding, the vertical direction is the direction of the wave propagation, see Fig.6. The procedure of measurement for Ti-6Al-4V alloy can be applied all along the entire cross-section of a target equal around 50 mm. In order to obtain a meaningful result for each cross-section of a fractured specimen more than hundred measurements should taken. A complete statistical analysis of the specimen relieves is out of scope of this Contract. A typical spall cross-section for armor steel Mars 190 with characteristic dimensions is presented in Fig.13, [1,28]. The length of horizontal segment ΔX_i, which the result of the first step of failure nucleation, is parallel to the impact plane. The length of vertical segment perpendicular to the impact plane is denoted by ΔY_i. This segment is produced later during plastic deformation by adiabatic shear banding. In order to develop a model for this new meso-mechanism it is important to determine the distribution of ΔX_i and ΔY_i all along the entire cross section of a target. Normally, spalled cross-section is divided into ~100 segments with constant length of ~500 μm. Microscopic observation of each segment allows measuring all ΔX_i and ΔY_i lengths. This meso-mechanism of failure can be approximated by a mean elementary cell composed of an horizontal segment of average length $\overline{\Delta X_i}$, a vertical segment of average length $\overline{\Delta Y_i}$ and with an average width of adiabatic shear band δ in between two vertical segments, as it is shown in Fig.13. Although a complete spatial distribution of characteristic dimensions was not performed for Ti-6Al-4V alloy an order of the mean values respectively for ΔX and ΔY is ~50 μm and ~30 μm. It is clear that a sufficient amount of experimental evidence has now been gathered to confirm the scenario of spalling for hard metallic alloys which involve a series of events in the micro- and meso-scales. Such scenario can be applied directly to formulate a completely new model of spalling already published in [1, 28].

MODELING ON MESO-LEVEL

Nucleation

Since the microscopy observations indicate that the criterion for spalling based on the coalescence of micro-voids or micro-cracks and adiabatic shearing is applicable for the relatively hard alloys, it is assumed that the new model based on the elementary cell can be also applied for Ti-6Al-4V. The first step for an elementary cell model shown in Fig.13 is nucleation of a micro-crack which starts when the local stress exceeds the local critical stress, σ_d, that is the stress leading to scenario shown in Figs 9, 10 and 11. The final result is shown in Fig.12. In a preliminary approach, the concept of elastic brittle fracture proposed by Griffith, and generalized to metals by adding to the elastic surface energy γ_e a supplementary surface energy γ_p of plastic

separation, thus $\gamma_R = \gamma_e + \gamma_p$ has been applied in modeling. The critical normal stress σ_d id given by

$$\sigma_d = \sqrt{\frac{\xi E \gamma_R}{(1-\nu^2)a_c}} \tag{1}$$

where $\xi = \pi/2$ for a penny-shape and $\xi = 2/\pi$ for a plane crack, E is the Young's modulus (E = 115.7 GPa), ν is the Poisson's ratio (ν = 0.331), $2a_c$ is the length of micro-crack and $\gamma_R = \gamma_e + \gamma_p$ is the surface fracture energy ($\gamma_e = 10^{-6} J/mm^2$ for steels, [40,41]. Values of E and ν are given after [35]. When a micro-crack nucleates, its tips propagate next with a high velocity under action of a decreasing stress, up to a final length a_c. According to Orowan, [41], the surface energy of plastic deformation in metals is approximately three orders of magnitude higher than the elastic surface energy. It can be assumed in the present analysis that the plastic surface energy is proportional to the elastic surface energy:

$$\gamma_p = \chi \gamma_e \tag{12}$$

where χ is the coefficient of proportionality. It is usually assumed that $\chi \cong 1000$. The approach assumed here neglects completely dynamics, however, because of a small dimension of such micro-crack, the inertia effect seems to be negligeable. Of course, a more complex approach can be invoked, but at this preliminary stage of modeling simplicity is an asset.

Crack propagation

Under the effective local stress σ_d, which is assumed constant, the micro-crack propagates at velocity $\dot{a}$ up to attainment its final length a_c. In the limit the following relation holds

$$2\,a_c = \overline{\Delta X_i} \tag{13}$$

It is assumed further that the propagation velocity $\dot{a}$ is constant. After [42] and [43], the limit velocity of crack propagation is between $0.4C_2$ and $0.6C_2$, where C_2 the speed of elastic shear waves. For Ti-6Al-4V alloy theoretical value of the speed of elastic shear waves is C_2 = 3.13 mm/μs. A more general discussion of moving cracks has been reviewed by [44]. In the case of Ti-6Al-4V an estimate of the crack speed is within the limits: 1250 m $s^{-1} \le \dot{a} \le$ 1880 m s^{-1}. However, the real velocity of a moving crack is much lower than those limits due to formation of a plastic zone in the crack tip, [44-46].

The propagation time over the distance a_c is given by the relation

$$t_d^* = \frac{\overline{\Delta X_i}}{2\dot{a}} \tag{14}$$

This time interval is relatively short, even for crack velocities propagating at a small fraction of the elastic wave speed. However, the normal stress may reach locally a quite high values.

Growth and coalescence by ASB

This stage absorbs more energy to be advanced and much longer time is required than the nucleation and propagation stages. Under tension load, the plastic deformation is localized within a small shear zone between two neighboring micro-voids or micro-cracks situated on different levels. In this way a high local shear stress is developed. Evolution of the shear stress in this zone has a typical evolution history for ASB as discussed by [12,38]. It is assumed in this stage of the modeling that plastic deformation in the fully formed micro-shear band, [47], increases abruptly up to the critical value Γ_c , from that instant the progressive cracking of the micro-shear band starts. In other terms, the vertical segment $\overline{\Delta Y_i}$ is rupturing within the core of the micro-shear band of thickness δ , and the failure begins from the critical value of shear deformation Γ_c. The progressive cracking of the ASB is continued at constant velocity V (close to the mass velocity of the reflected wave) until a complete coalescence of two neighboring micro-cracks. The plastic deformation in the shear band is given by the relation:

$$\Gamma_p = \frac{Vt^*}{\delta} \tag{15}$$

and the strain rate is given by

$$\dot{\Gamma}_p = \frac{V}{\delta} = cons\tan t \tag{16}$$

It is possible to distinguish three stages in development of the ASB on the strain hardening curve, $\tau(\Gamma)$, where τ is the shear stress, [38]. The first stage is finished when the shear stress reaches a maximum. The second corresponds to a slight decreasing of stress where deformation becomes inhomogeneous and localization begins. The last one corresponds to a rapid stress decrease which signals a rapid localization of shear deformation, the ASB is fully formed.. The substantial growth of cavities occur during the second stage and the coalescence of neighboring micro-cracks occurs only during stage three. In order to determine evolution of the shear stress inside the ASB, in the model only the third stage is considered, that is the final localization, where the shear stress decreases rapidly with time, [47].

The evolution of shear stress τ is calculated for a plastic material with the linear thermal softening proportional to the homologous temperature, and with the constant rate sensitivity index m, by using of the following constitutive relation

$$\tau\left(\dot{\Gamma}_p, T\right) = \tau_0\left(1 - a\frac{T}{T_m}\right)\left(1 + b\frac{\dot{\Gamma}_p}{\dot{\Gamma}_0}\right)^m \tag{17}$$

where T_m is the melting temperature in Kelvins ($T_m \approx 1900$ K), and T is the current temperature, Γ_p is the shear strain rate of plastic deformation, $\dot{\Gamma}_0$ (s^{-1}) is the reference strain rate, a is the temperature sensitivity coefficient, b is the rate sensitivity coefficient, and τ_0 (MPa) is the threshold stress. Some constants, more exactly a, b and m, can be determined for Ti-6Al-4V by simple tension or compression tests at different strain rates and temperatures. For example, value of shear stress τ_0 can be estimated from [9] as $\tau_0 \approx 1100$ MPa at shear strain rate $\sim 2x10^4\ s^{-1}$.

The uniform heating due to plastic deformation can be calculated with the following thermodynamic relation

$$\frac{dT_{uni}}{d\Gamma_p} = \frac{\beta}{\rho C_v}\tau\left(\dot{\Gamma}_p, T\right) \tag{18}$$

where $\beta = 0.9$ is the Taylor-Quinney coefficient, the density in RT is $\rho = 4430\ kg/m^3$, and the specific heat at constant volume is $C_v = 543$ J/(kg K). The optical microscopy observations of the shear bands in Ti-6Al-4V have allowed for an estimation of the final localization strain. It appears that instability and formation of inhomogeneous deformation occurs approximately at plastic shear strain equal approximately to $\Gamma \approx 0.011$ at strain rate $\sim 10^4\ s^{-1}$, [9]. By assuming that shear strain rate is constant during the period of shear deformation, for example $\dot{\Gamma}_p = 10^6 s^{-1}$, calculations using Eq.(7), and Eq.(8) yield the temperature increase ~100 K.

Beginning from the third stage which starts at the temperature level ~100 K, the adiabatic rise of temperature continues inside the ASB due to continued strain localization, this stage is determined by the following relation

$$\frac{\Delta T_{adia}}{\Delta\Gamma_p} = \frac{\beta}{\rho C_v}\tau\left(\dot{\Gamma}_p, T\right) \qquad \Delta T_{adia} = T_{adia} - T_{uni} \tag{19}$$

After integration of Eq.(9) the evolution of temperature at this stage is found as follows

$$\Rightarrow T_{adia} = \frac{T_m}{a}\left[1 - \left(1 - a\frac{T_{uni}}{T_m}\right)\exp\left\{-\frac{a}{T_m}\frac{\beta\kappa_0}{\rho C_v}\left(1 + b\frac{\dot{\Gamma}_p}{\dot{\Gamma}_0}\right)^m\left(\Gamma_p - \Gamma_{loc}\right)\right\}\right] \tag{20}$$

For large plastic deformation in shear an increase of temperature usually obtained is a high fraction of the melting point. It is then acceptable to neglect the temperature increase due to

uniform plastic deformation and also during the coalescence stage. In the following part of the modeling only adiabatic evolution of temperature in the core of the ASB is considered. By assuming that the strain rate is constant the increment of plastic strain in the ASB can be written as:

$$d\Gamma_p = \dot{\Gamma}_p dt \tag{21}$$

By substituting Eq.(10) into Eq.(7), and by integrating of Eq.(11) with the following limit conditions,

If $t = 0$ then $T = T_{uni} = T_0 + \Delta T_{uni}$

If $t \to \infty$ then $\tau \to 0$,

the final expressions are obtained for temperature and shear stress evolution in time

$$T(t) = \frac{T_m}{a}\left[1 - \left(1 - a\frac{T_{uni}}{T_m}\right)\exp\left(-\frac{a}{T_m}\omega t\right)\right] \tag{22}$$

$$\tau(t) = \tau_0\left(1 - a\frac{T_{uni}}{T_m}\right)\exp\left[-\frac{a}{T_m}\omega t\right]\left(1 + b\frac{\dot{\Gamma}_p}{\dot{\Gamma}_0}\right)^m \tag{23}$$

with the following parameter

$$\omega = \frac{\kappa_0 \beta}{\rho C_V}\left[1 + b\frac{\dot{\Gamma}_p}{\dot{\Gamma}_0}\right]^m \dot{\Gamma}_p$$

where T_{uni} is the initial temperature of shear band at the beginning of the third stage, T_0 is initial temperature of the material. Finally, all these simplifications and derivation steps has allowed to define the new model for the one mean cell. The model permits to estimate the evolution of the mean normal stress as a function of time or the spall opening in the meso level. All stages of the modeling are included into Table 3. Where in this Table S_{pl} is the elementary surface on which the shear stress is applied. It is also assumed that this area is a square of $\overline{\Delta Y_i}$ side. The local mean meso-stress vs. time can be estimated by application of this model, the final result is shown schematically in Fig.14. Since the assumed thickness of the ASB is usually small the stage 2 is the shortest. The longest one is the number 3 where the shear failure propagates in the core of ASB. It occurs in proportion to the velocity of material separation. In the analysis of the normal meso-stress, a pseudo 3D analysis was applied, that is the elementary cell was assumed as symmetric in the X and Z directions, where the (X, Z) plane is parallel to the spall surface. So the elementary cell shown in Fig.13 for the X direction is the same in the Z direction. But the crack is assumed as propagating only in the X direction (plane strain). This inconsistency will be studied in the future. The modeling presented here is the preliminary stage especially having in mind direct application to Ti-6Al-4V alloy.

In order to estimate the macro or global stress level for spalling predicted by this model, and compare in the future with experimental results, the definition of the mean value of the integral can be applied

$$\sigma_F = \frac{1}{\Delta t}\int_{t_0}^{t_m} \sigma_{meso}(t)dt$$

where $\Delta t = t_m - t_o$ is the time interval of integration. The longest interval is, of course, between the instants when the micro-crack starts to propagate, $t_o = 0$, and it ends at the moment of the complete separation, when the normal meso-stress is zero. However, due to the fact that the final instants of separation lead to a relatively low values of the mean stress, the interval of integration should be assumed as a parameter, and the integration should be performed with shorter values of Δt. The variation of the integration period should be limited only to the stage 3. This cut-off procedure fits the global failure stress to experimental level. However, the procedure is artificial and further studies are necessary to clarify the main cause of this discrepancy. The mean spall stress σ_F is in general lower when integration is performed till the end of the stage 3 as compared with the experimental values [1,28]. In spite that the spall stresses obtained via the model are as a rule lower than expected, the trend, however, is correct, there is a stress-dependent fracture delay time that decreases with increasing stress. There are many physical reasons why such difference has occurred, it is prematurely to discuss them. One possibility is to introduce in the model a notion of the threshold stress, [28].

CONCLUSIONS

Spall strength of titanium alloys was recently reported in many publications. Although in some publications the spall strength is given not often a data are not complete. It causes that comparison of particular results are very frequently not so simple. It is out of scope of this Report to review available experimental data for titanium alloys, including Ti-6Al-4V alloy, but some of results published recently will be mentioned.

A series of spall tests for four Russian Ti alloys VT-6, VT-14, VT-20 and VT-23 was reported in [48] . It was found that the free surface velocity profiles display forward $\alpha \rightarrow \omega$ and reverse $\alpha \rightarrow \omega$ phase transition in all those alloys. But the most important finding from the point of view of this study was confirmation of shear zones and adiabatic shear bands situated in parallel direction to the propagation direction of plane waves. Those adiabatic shear bands end with micro-cracks on each side. It was also shown in this study that the shear bands had a very complicated internal microstructure. The phase transformation change a normal dependence of the spall strength versus impact velocity showing a decrease when the impact velocity reaches certain level. Typical values of the spall strength at low impact velocities ~ 400 m/s $< V_0 <$ ~450 m/s, varies for all four alloys within the following limits : ~4.4 GPa $< \sigma_F <$ ~4.9 GPa . When the velocity range is ~500 $< V_0 <$ ~600 m/s the spall strength drops for all alloys to ~4.0 GPa.

Is study reported in [36] the spall strength was determined for Ti-6Al-4V alloy at different temperatures from RT to ~790 K. Unfortunately, the spall strength in RT was not determined (value of 5.0 GPa was assumed after Me-Bar et al., (1987)). The same $\alpha \rightarrow \omega$ phase

transformation was mentioned. It is interesting to note that the spall strength drops to value ~4.3 GPa at $T \approx 790$ K.

A more recent study on spall strength of four Ti-6Al-4V alloys with different grain size and oxygen content was reported in [39]. Two of those alloys had different microstructure and grain sizes, 14 μm and 810 μm. The second two alloys had different oxygen content, 0.105 % and 0.198 % . It was found that the oxygen influences the spall strength via intensity of reverse $\omega \rightarrow \beta$ transformation. When a phase transformation occurs typically the spall strength decreases with the impact velocity. Since in this study the impact velocities were the lowest possible to obtain the incipient spall level , from 290 m/s to 460 m/s, only results for the lowest impact velocities given in [Mesch+Goo] are discussed below. For all four alloys tested at the range of low impact velocities, ~440 m/s < V_0 < ~460 m/s, the spall strength varied within the following limits 4.5 GPa < σ_F < 5.0 GPa . Those values are very close to our values shown in Fig.5 and Table 2. Since in the discussed paper the flyer thickness is not given, thus the impulsion time is unknown, a more exact comparison with present results is impossible. Values of the spall strength given above fit the region of the critical time $t_C \approx 2.0$ μs in Fig.5.

Experiments performed earlier on hard metallic alloys like aluminum 7020-T6 and armor steel Mars 190 have reviled the mechanism of spalling which combines in the meso-level a quasi-brittle initiation of micro-cracks or micro-voids and later a coalescence by adiabatic micro-bridges in the form of adiabatic shear bands, [1]. Such mode of spalling was also reported earlier, for example [30], also [48]. Plane micro-cracks and voids are nucleated by hard particles, and in the present case by α-β grain boundaries and triple points, Figs 9 to 12.. Spatial distribution of inhomogeneities constitutes a very important statistical factor in fracture, and in particular in fracture dynamics. This statistics are reflected in SEM observations of segment distribution on the spalled surface, such as shown in Fig.6.

The mean values of the steps observed on specimen cross sections, Fig.6, could serve to calibrate the new model of spalling based on brittle fracture initiation, adiabatic shearing and failure of ASB. The model should predict correctly the expected trends, that is the critical normal stress for spalling is history-dependent, with increasing stress the delay time for fracture decreases. Of course, a phase transition could change this scenario. A global cumulative criterion based on this principle has been introduced and discussed earlier, [1,22,23]. The constants in this failure criterion have been found and the solid line in Fig 5 represents fit to experimental data. Further studies are of great importance, especially to correlate for the same material the minimum spall strength on the incipient level obtained by the acoustic approximation and by measurement of the free surface velocity . Since the spalling process depends on time-dependent defect accumulation in adiabatic conditions, an increase of impact velocity of flyer should change the resulting value of the spall stress. This is one of reasons why the spall strength may differ for the same material when conditions of experiment are not the same, for example the rise time and pulse duration as well as its amplitude. Again, a material must be metallurgically stable. Different impact velocity of the flyer related directly to the pulse amplitude may also change the micro-mechanism of material separation on the meso-level. For example, the picture shown in Fig.6 may change when the impact velocity is substantially increased. This will probably occur due to a phase transformation. Another factor to be studied, in relation the micro-mechanics of failure, is the rise time of the incident wave. The rise-time is closely related to the length of the reflected tensile wave causing spalling. Finally, very frequently in studies of spalling at higher impact velocities, say 500 m/s and higher the thermal coupling via plasticity is neglected. This causes not so exact interpretation of results.

The conditions of the experiment and results for Ti-6Al-4V reported here are well defined and they should be compared with data obtained in similar conditions.

ACKNOWLEDGEMENT

The research reported herein has been sponsored in part by the United States Army through its European Office and in part by CNRS – France. Fruitful discussions with Dr. W. A. Gooch at the initial stages of the Contract are also acknowledged. Spall specimens were prepared by the Army Research Laboratory, AMSRL-WM-TA, Aberdeen Proving Ground, MD, USA.

REFERENCES

[1] P.Chevrier and J.R.Klepaczko, Fracture model for spalling of hard metallic materials based on the meso-scale approach, in: Fundamental Issues and Application of Shock-Waves and High Strain Rate Phenomena, Proc. Int. Conf. EXPLOMET 2000, Elsevier (2000).

[2] P.Chevrier and J.R.Klepaczko, Spall fracture: Mechanical and microstructural aspects, Eng. Fract. Mech., 63 (1999), pp. 273-294.

[3] G.Taylor, The use of flat-ended projectiles for determining dynamic yield stress, Theoretical considerations, Proc. Roy. Soc., London, **A194** (1948), 289.

[4] A.C.Whiffin, The use of flat-ended projectiles for determining dynamic yield stress, Tests on various metallic materials, Proc. Roy. Soc. , London, **A194** (1948), 300.

[5] J.R.Klepaczko, An experimental technique for shear testing at high and very high strain rates. The case of a mild steel, Int. J. Impact Engng., 15 (1994), pp. 25-39.

[6] T.Nicholas and S.J.Bless, High strain rate testing, in Metals Handbook Ninth Edition, Mechanical Testing, **8** (1985), 208.

[7] K.S.Kim and R.J.Clifton , Pressure-shear of 6061-T6 aluminum and alpha titanium, J. Appl. Phys., **47** (1980), 11-16.

[8] J.R.Klepaczko, Effects of Impact Velocity and Stress Concentrators in Titanium on Failure by Adiabatic Shearing, Final Technical Report for the US Army ERO, Contract DAJA 49-90-C-0052, LPMM, Metz University, (1998).

[9] J.R.Klepaczko, Behavior of Ti-6Al-4V alloy at high strain rates, Proc. Int. Conf. DYMAT 2000, J.de Physique, Coll. C9 (2000).

[10] R.Dormeval and J.P.Ansart, Adiabatic shearing: effect of pre-straining, Proc.Conf. DYMAT 85, J. de Physique, Coll. C5, Appendix No 8, 46 (1985), pp. C5-299 -C5-306.

[11] L.W.Meyer, L.Krueger, W.A.Gooch and M.S.Burkins, Analysis of shear band effects in titanium relative to high strain-rate laboratory/ballistic impact tests, Proc. Int. Conf . EURODYMAT 97, J.de Physique IV, (1997).

[12] J.R.Klepaczko and B.Rezaig, A numerical study of adiabatic shear banding in mild steel by dislocation mechanics based constitutive relations , Mechanics of Materials, 24 (1996), pp.125-139

[13] P.Chwalik and J.R.klepaczko, High strain rate shear testing of Ti-6Al-4V alloy, Materials Sci. and Engng, (2003), accepted.

[14] J.R.Klepaczko, Stress concentrators and rate effects in formation of adiabatic shear bands, Technical Report prepared for the US Army European Res. Office, Contract DAJA N68171-95-C-9071, LPMM, Metz University (1996).

[15] M.Klosak and J.R.Klepaczko, Numerical study of the Critical Impact Velocity in shear, Appendix N0 1, Final Technical Report prepared for the US Army European Res. Office, Contract DAJA N68171-95-C-9071, LPMM, Metz University (1996)

[16] W.Gooch, M.S.Burkins, H.J.Ernst and T.Wolf, Ballistic performance of titanium against laboratory penatrators with aspect-ratio of 10 or grater, Proc. of the 15th Int. Ballistic Symp. (1995).

[17] W.Gooch, M.S.Burkins, H.J.Emst and T.Wolf, Ballistic penetration of titanium alloy Ti-6AL-4V, Proc. of the Lightweight Armour Systems Symp., The Royal Military College of Science, Shrivenham, Swindon, England (1995).

[18] W.Gooch, MS. Burkins and K.Frank, Ballistic performance of titanium against laboratory penetrators, Preprint of the Proc. of the 1-st Australasian Congress on Appl. Mech'96, Melbourne, Australia (1966).

[19] T.G.Farrand, Various target material failure mechanisms observed for ballistic penetrators, Rep. BRL-TR-3255, (Aug. 1991).

[20] I.V. Varfolomeyev and J.R.Klepaczko, Approximate analysis on strain rate effects and behavior of stress and strain fields at crack tip in Mode II in metallic materials, Appendix No 1 to the Technical Report prepared for the US Army European Res. Office, Contract DAJA 45-90-C-0052, LPMM, Metz University (1992).

[21] I.V. Varfolomeyev and J.R.Klepaczko, Effect of deformation rate on Mode II crack tip plastic zone geometry , Problemy Prochnosti (Strength of Materials), N03 (1995), pp.46-55.

[22] J.R.Klepaczko, Dynamic crack initiation, some experimental methods and modeling, in: Crack Dynamics in Metallic Materials, Springer Verlag, Vienna (1990).

[23] S.Hanim and J.R.Klepaczko, Numerical study of spalling in an aluminum alloy 7020-T6, Int. J. Impact Engng, 22 (1999), p.649.

[24] J.R.Klepaczko, Plastic shearing at high and very high strain rates, Proc. Int. Conf . EURODYMAT 94, J. de Physique IV, Coll. C8, 4 (1994), pp.C8-35 - C8-40.

[25] J.R.Klepaczko, Recent progress in testing of materials in impact shearing , Proc.of theJoint ASME/JSMIE Pressure Vessels and Piping Conf PVP-Vol.300, Dynamic Fracture, Failure and Deformation, ASME (1995), pp. 165-173.

[26] J.R.Klepaczko, Experimental investigation of adiabatic shear banding at different impact velocities, Final Technical Report for the US Army European Res. Office, Contract DMA

[27] B.Etcheverry, Microstructure et ecaillage du Ti-6Al-4V, DEA-MMSP, Laboratoire de Physique et Mécanique de Matériaux, Université de Metz, Metz, (2003).

[28] J.R.Klepaczko and P.Chevrier, A meso-model of spalling with thermal coupling for hard metallic materials, Engng Fract. Mech., **70** (2003), 2543.

[29] P.Chevrier, and J.R.Klepaczko, Discussion of fracture criteria in spall mechanics, Engng. Trans., 45 (1997), 47.

[30] D.R.Curran, L.Seaman and D.A.Shockey, Dynamic failure of solids, Physics reports 147, North-Holland, Amsterdam, 1987, **5-6**, 253-388.

[31] A.N.Dremin and A.M.Molodets, On the spall strength of metals, Proceedings of the Int. Symp. on Intense Dynamic Loading and its Effects, Beijing, Pergamon Press, (1986), 13-22.

[32] S.N.Zhurkov, Kinetic concept of the strength of solids, Int..J. Fracture, 1 (1965), 311-323.

[33] T.Yokobori, The Cottrell-Billy theory of yielding of iron, J. Appl. Phys. (Letters), **23** (1952), 1423.

[34] H.Conrad, Thermally activated deformation in metals, J. of Metals, **16** (1964), 582.

[35] H.R.Arrieta, Dynamic Testing of Advanced Materials at High and Low Temperatures, M.S. Thesis, Pardue University, (1999).

[36] H.V.Arrieta and H.D.Espinosa, The role of thermal activation on dynamic stress-induced inelasticity and damage in Ti-6Al-4V, Mech. of Materials, **33** (2001), 573-591.

[37] H.C.Rogers, Adiabatic plastic deformation, Ann. Rev. Mat. Sci., **9** (1979), 238-311.

[38] A.Marchand and J.Duffy, An experimental study of the formation process of adiabatic shear bands in structural steel, J. Mech. Phys. Solids, **36** (1988), 251.

[39] Yu.I.Mescheryakov, N.I.Zhigacheva, A.K.Divakov, Yu.A.Petrov and W.A.Gooch, Spall strength of Ti-6Al-4V titanium alloy of varying heat treatment and content of oxygen, Inst. Probl. Of Mech. Engng, RAS, St. Petersburg, (2003).

[40] E.Orowan, Energy criteria of fracture, Welding J., **34** (1955), 1575.

[41] E.Orowan, Fracture and strength of solids, Reports in Physics, **XII** (1948), 185.

[42] E.H.Yoffe, The moving Griffith crack, Phil. Mag., **42** (1951), 739.

[43] K.B.Broberg, The propagation of brittle crack, Arkiv for Fysik, **18** (1960), 159.

[44] L.B.Freund, Dynamic Fracture Mechanics, Cambridge University Press, Cambridge, UK (1989).

[45] G.Hudson and M.Greenfield, Speed of propagation of brittle cracks in steel, J. Appl. Phys., **18** (1947), 405.

[46] D.S.Dugdale, Yielding of steel sheets containing slits, J. Mech. Phys. Solids, **8** (1960), 100.

[47] T.W.Wright and H.Ockendon, A model for fully formed shear band, J. Mech. Phys. Solids, **40** (1992), 1217.

[48] M.Zhou and R.J.Clifton, Dynamic ductile rupture under conditions of plane strain, Int. J. Impact Engng, **3** (1997),189-206.

TABLES

Table 1 Specimen dimensions for plate impact experiments

Table 2 Results of plate impact experiments

Table 3 Three phases of failure in the meso-model of spalling

FIGURE CAPTIONS

Fig.1 Layout of plate impact experiment, bore diameter 57 mm.

Fig.2 Schematic result of spall experiment in the form of $\sigma_F(t_C)$, σ_{F0} denotes the threshold stress.

Fig.3 Initial microstructure along rolling direction for Ti-6Al-4V alloy, [27].

Fig.4 Initial microstructure perpendicular to the rolling direction for Ti-6Al-4V alloy, [27].

Fig.5 Final result of spall experiments for Ti-6Al-4V in the form $\sigma_F(t_C)$, the solid line represents the global model of failure.

Fig.6 Profile of fracture surface for Ti-6Al-4V alloy, $V_0 = 370$ m/s, $t_C = 1.9$ μs.

Fig.7 SEM profile showing initial stage of material separation, micro-cracks and shearing.

Fig.8 SEM profile showing final stage of separation, that is complete separation.

Fig.9 Initial micro-voids in Ti-6Al-4V loaded by plane wave, upper photo: micro-cavities on phase boundaries, lower: mico-cavity in the grain boundary, [35,36].

Fig.10 Micro-voids in the initial stage of failure localized in the interface α/β , direction parallel to the wave front, [27].

Fig.11 Micro-voids in the initial stage of failure localized in junctions of the α/β phase, [28].

Fig.12 Micro-crack perpendicular to the lamellae direction, [28].

Fig.13 Mode of failure for hard metallic materials with ΔX_i and ΔY_i segments, the lower part shows the elementary cell, material: Mars 190, [1].

Fig.14 Schematic evolution of the normal stress as a function of time during three stages of Failure, see also Table 3, [1].

- **Table 1 :**

N°	Target thickness [mm]	Flyer thickness [mm]
Ti 2(1) 03	6	3
Ti 2(2) 03	6	3
Ti 3(2) 03	8	4
Ti 3(3) 03	8	4
Ti 4(2) 03	10	6
Ti 4(3) 03	16	6
Ti 4(4) 03	16	6
Ti 5(1) 03	16	8
Ti 5(3) 03	20	8
Ti 6(1) 03	20	10
Ti 6(2) 03	20	10

- **Table 2 :**

N°	Loading time [μs]	Impact velocity [$m.s^{-1}$]	Spall stress [GPa]	Damage level
Ti 2(1) 03	0.9	420	5.58	No spall
Ti 2(2) 03	0.9	429	5.70	Advanced spall
Ti 3(2) 03	1.3	460	6.11	Complete spall
Ti 3(3) 03	1.3	391	5.19	No spall
Ti 4(2) 03	1.9	370	4.91	Intermediate spall
Ti 4(3) 03	1.9	360	4.78	Intermediate spall
Ti 4(4) 03	1.9	348	4.62	Intermediate spall
Ti 5(1) 03	2.66	340	4.52	Intermediate spall
Ti 5(3) 03	2.66	322	4.28	Intermediate spall
Ti 6(1) 03	3.3	300	3.98	Incipient spall
Ti 6(2) 03	3.3	291	3.86	Incipient spall

Table 3

Triggering end propagation of micro-crack	
$0 \le t^* \le t_d^*$	$t_d^* = \dfrac{\overline{\Delta X_i}}{2\dot{a}}$
$\sigma^{méso} = \sigma_d$	$\sigma_d = \sqrt{\dfrac{E\xi\gamma_e(1+\chi)}{(1-\nu^2)(\overline{\Delta X_i}/2)}}$
Shearing	
$t_d^* \le t^* \le t_d^* + t_c^*$	$t_c^* = \dfrac{\delta\Gamma_c}{V}$
$\sigma^{méso} = \dfrac{F^{méso}}{S_{cellule}}$	$S_{pl} = \overline{\Delta Y_i}^2$
$F^{méso} = \tau(t^*)S_{pl}$	$S_{cellule} = \overline{\Delta X_i}^2$
	$\tau(t^*)$ (IV.13)
Fracturing of shear band	
$t_d^* + t_c^* \le t^* \le t_d^* + t_{max}^*$	$t_{max}^* = \dfrac{1}{V}\left[\delta\Gamma_c + \overline{\Delta Y_i}\right]$
$\sigma^{méso} = \dfrac{F^{méso}}{S_{cellule}}$	$S_{pl} = \left[\overline{\Delta Y_i} - V(t^* - t_c^*)\right]^2$
$F^{méso} = \tau(t_c^*)S_{pl}$	$S_{cellule} = \overline{\Delta X_i}^2$
	$\tau(t_c^*)$ (IV.13)

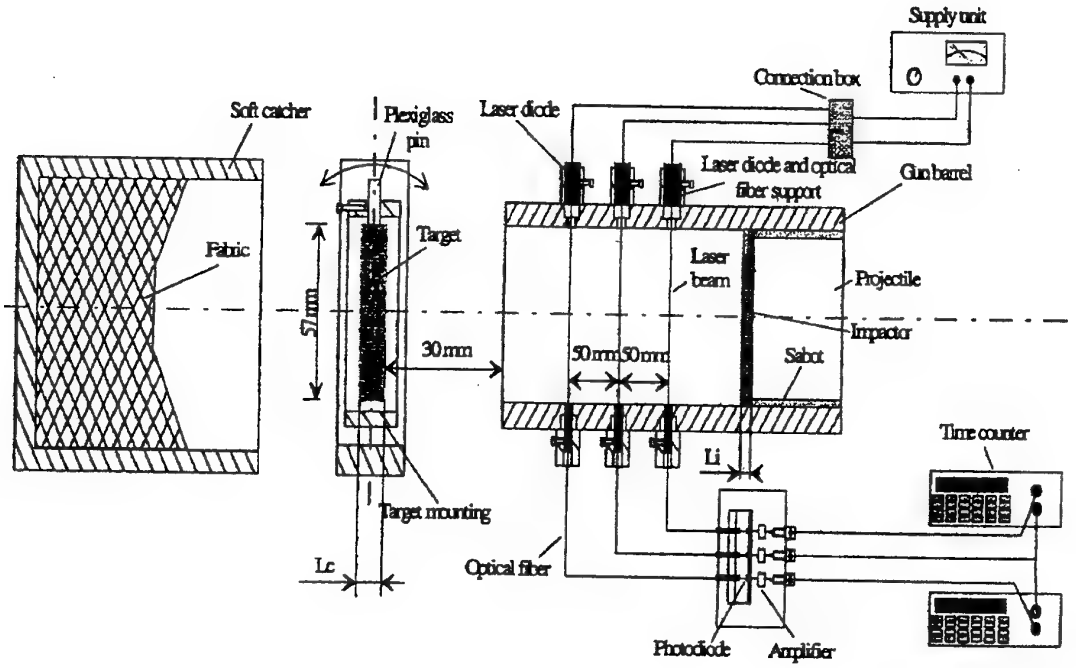
Supply unit
Connection box
Soft catcher
Plexiglass pin
Laser diode
Laser diode and optical fiber support
Gun barrel
Fabric
Target
Laser beam
Projectile
57 mm
Impactor
30 mm
50 mm
50 mm
Sabot
Time counter
Li
Target mounting
Lc
Optical fiber
Photodiode
Amplifier

Fig. 1

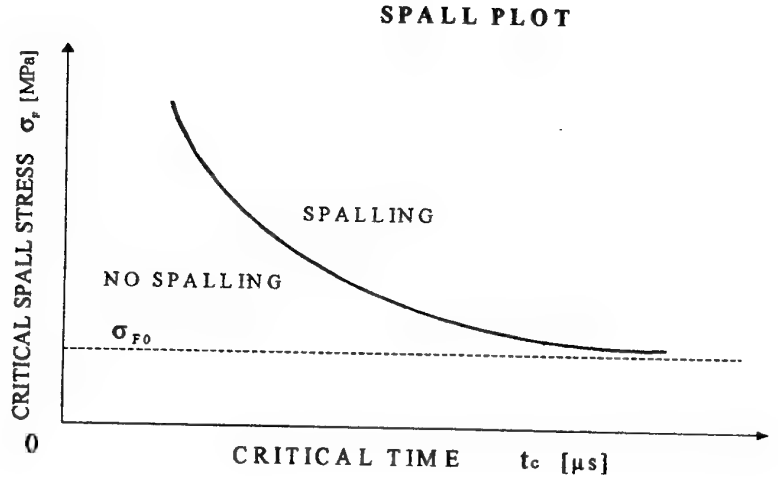
SPALL PLOT
CRITICAL SPALL STRESS σ_F [MPa]
SPALLING
NO SPALLING
σ_{F0}
0
CRITICAL TIME t_c [μs]

Fig. 2

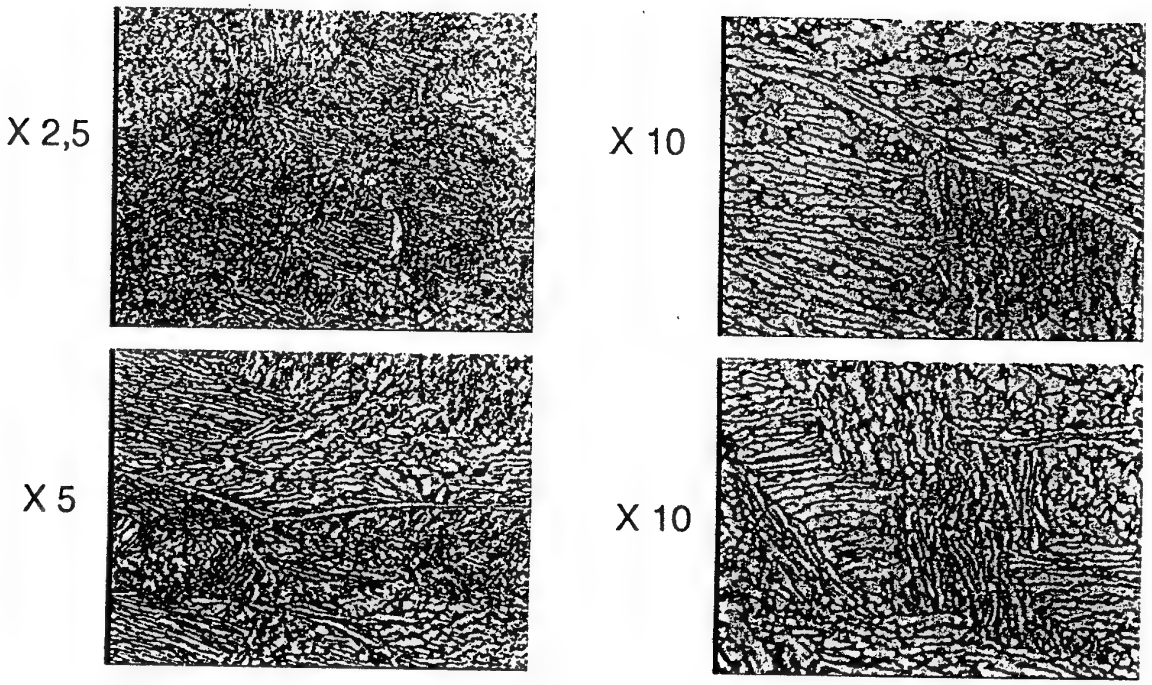

Fig. 3

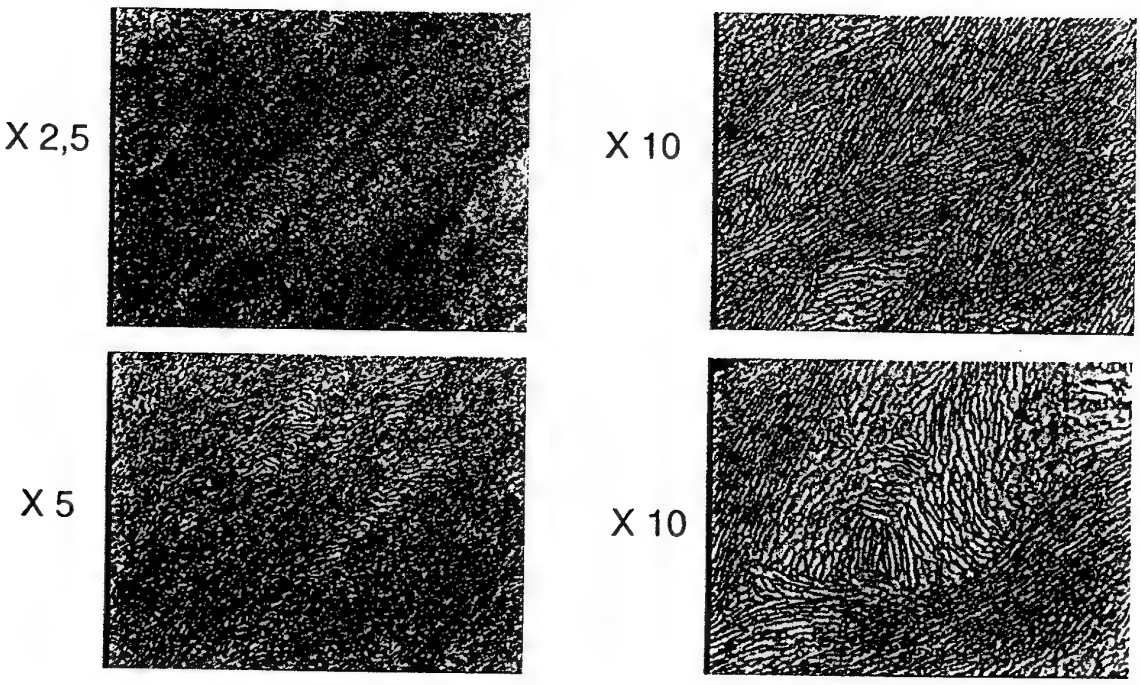

Fig. 4

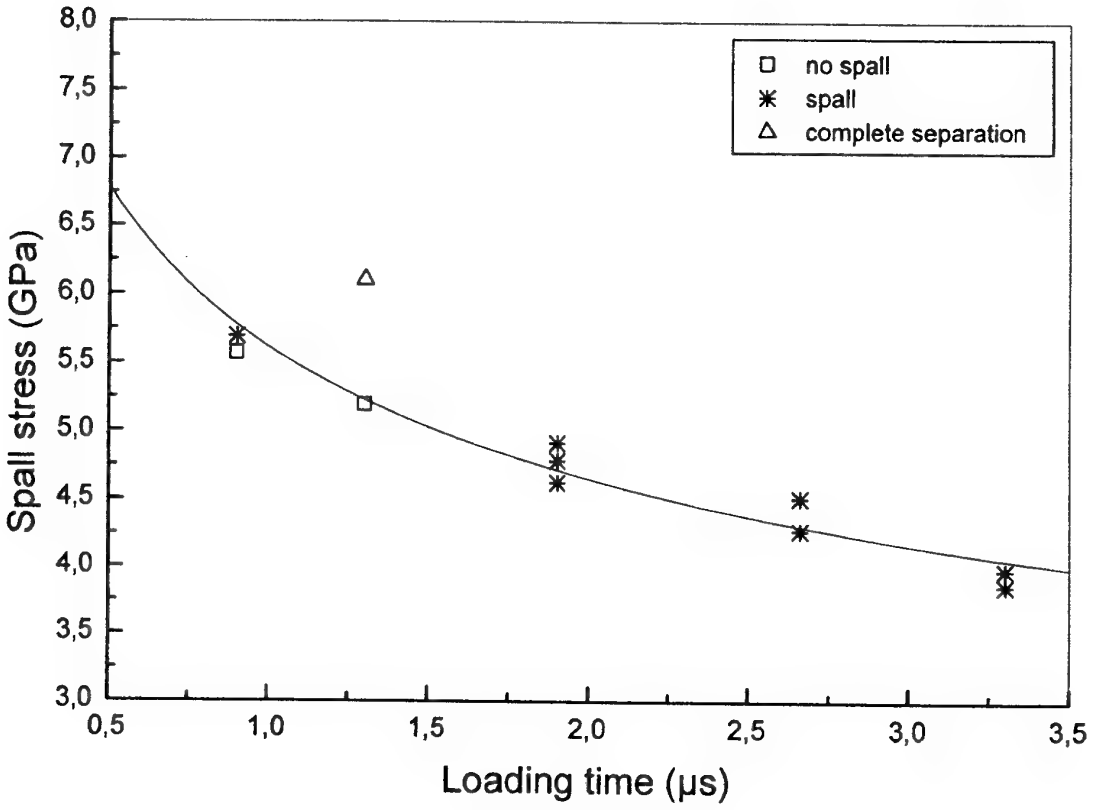
8,0
7,5
7,0
6,5
6,0
5,5
5,0
4,5
4,0
3,5
3,0
Spall stress (GPa)
0,5
1,0
1,5
2,0
2,5
3,0
3,5
Loading time (μs)
no spall
spall
complete separation

Fig. 5

Ti – 6Al – 4V

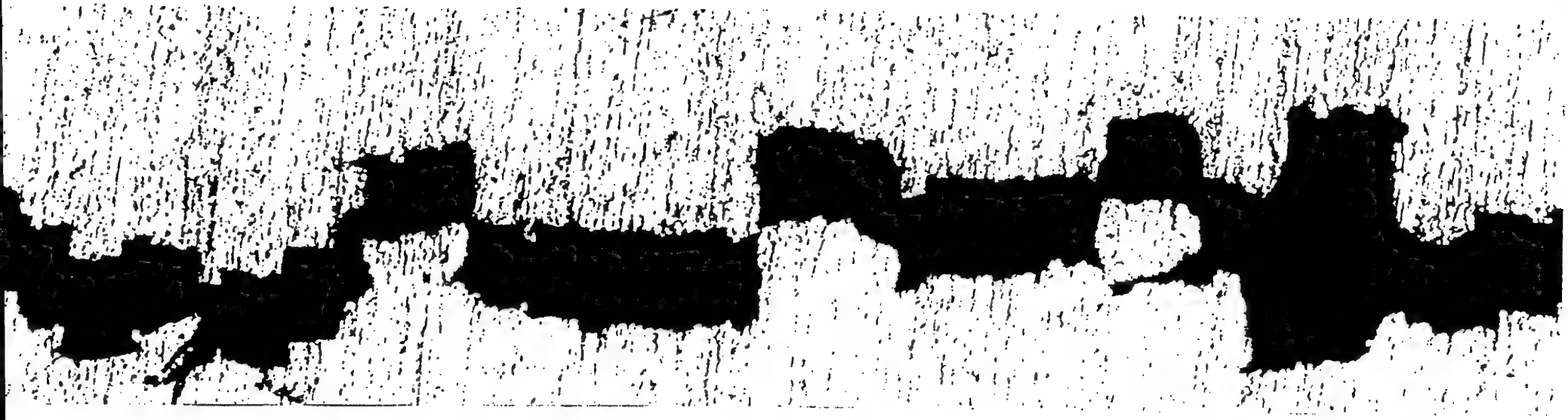

Impact velocity $V_0 = 370$ m/s
Critical time $t_C = 1.9$ μs

1.0 mm

Fig. 6

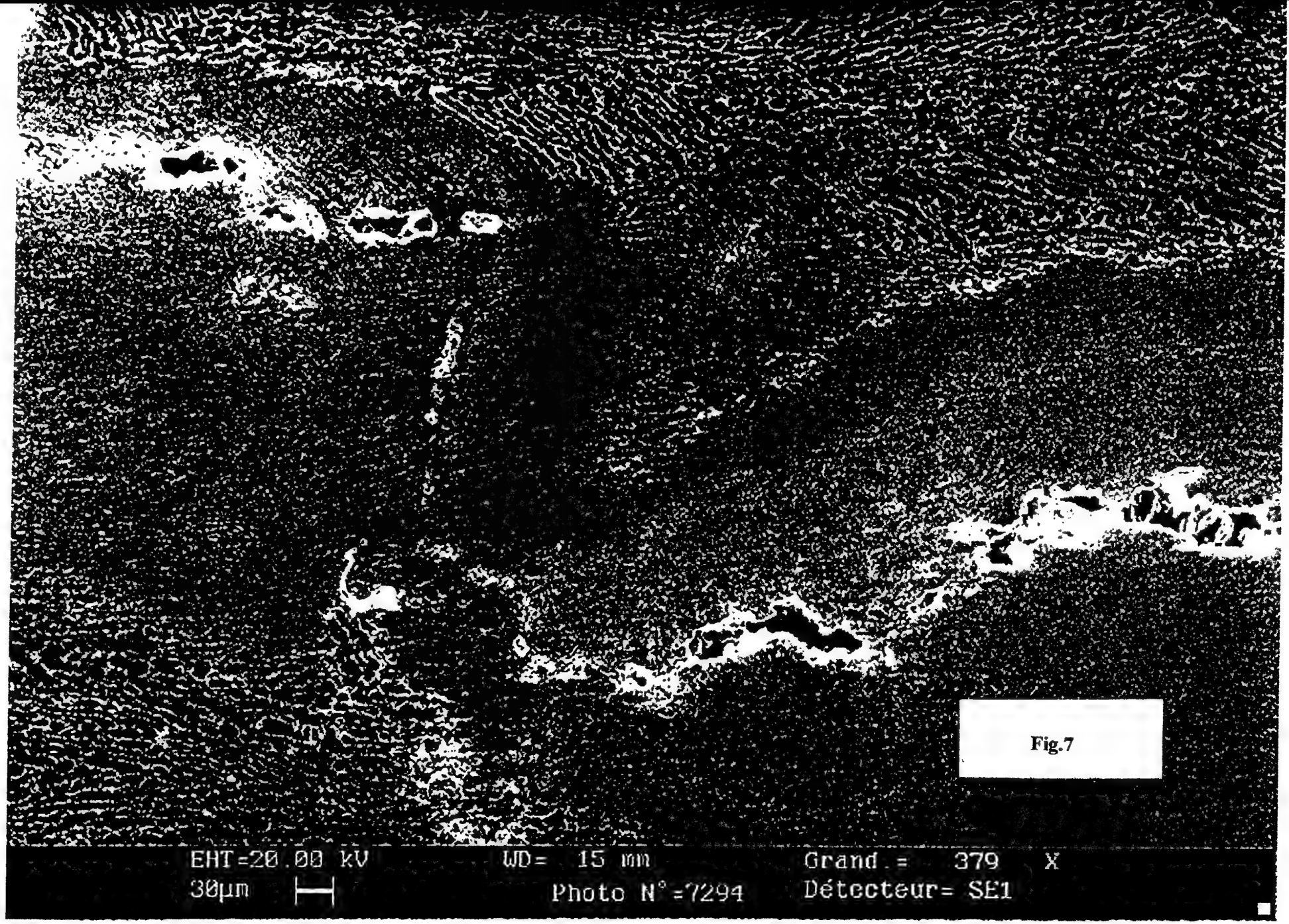
EHT=20.00 kV
WD= 15 mm
Grand.= 379 X
30µm
Photo N°=7294
Détecteur= SE1

Fig.7

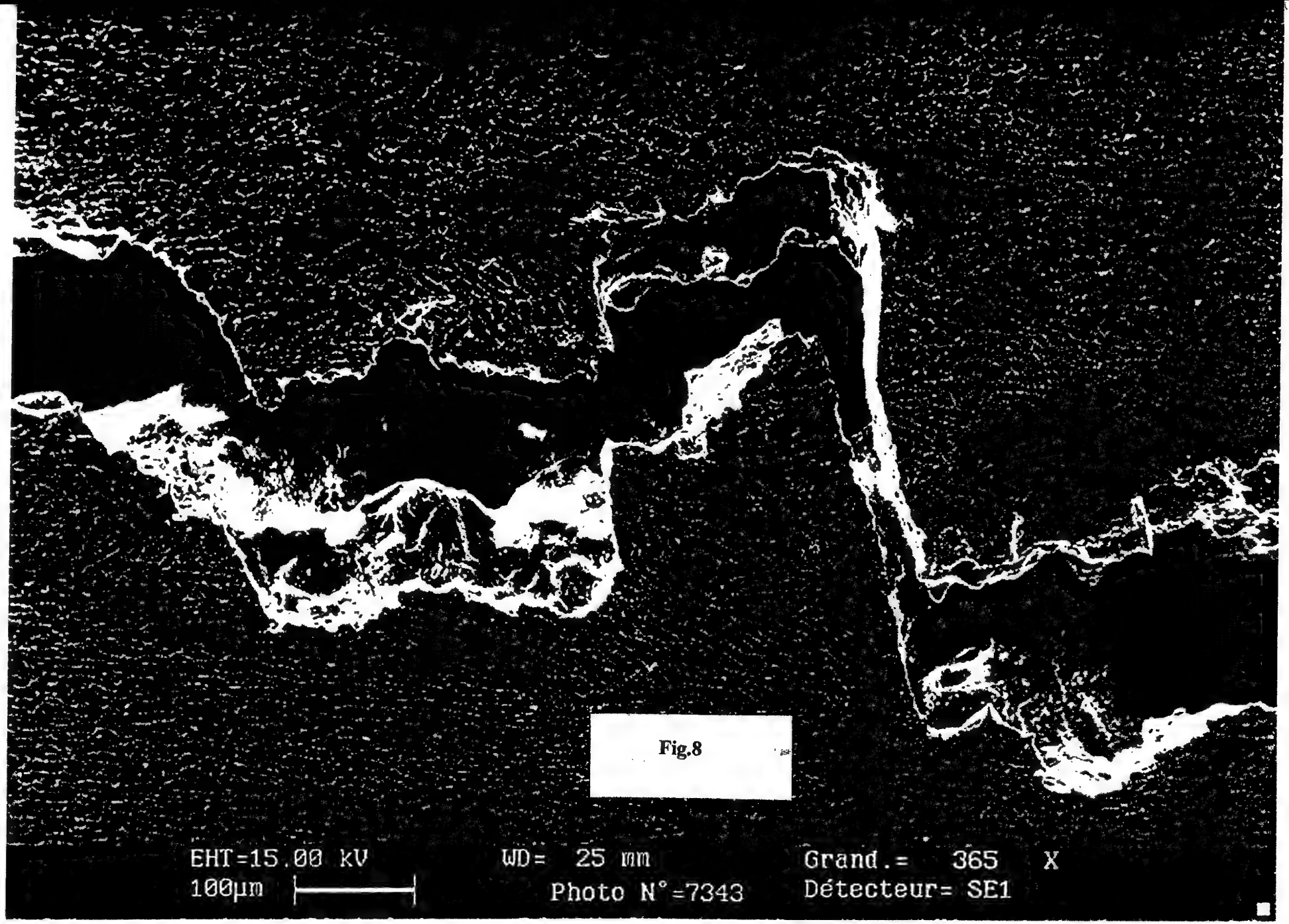
EHT=15.00 kV
WD= 25 mm
Grand.= 365 X
100µm
Photo N°=7343
Détecteur= SE1

Fig.8

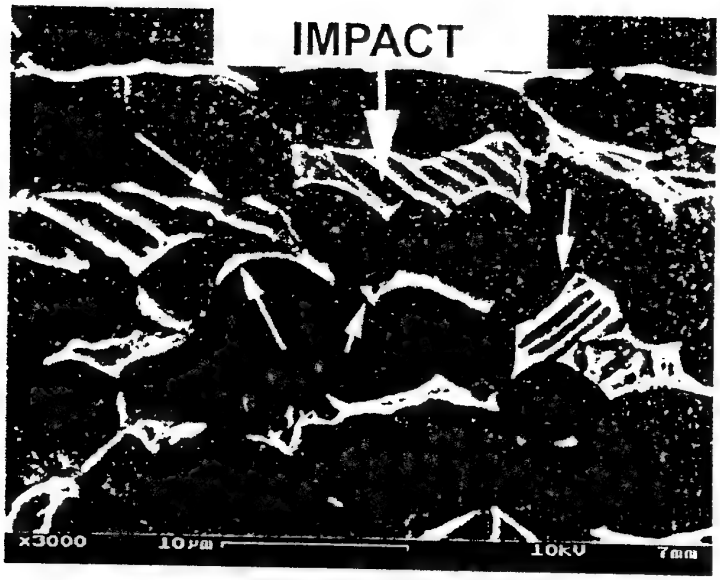

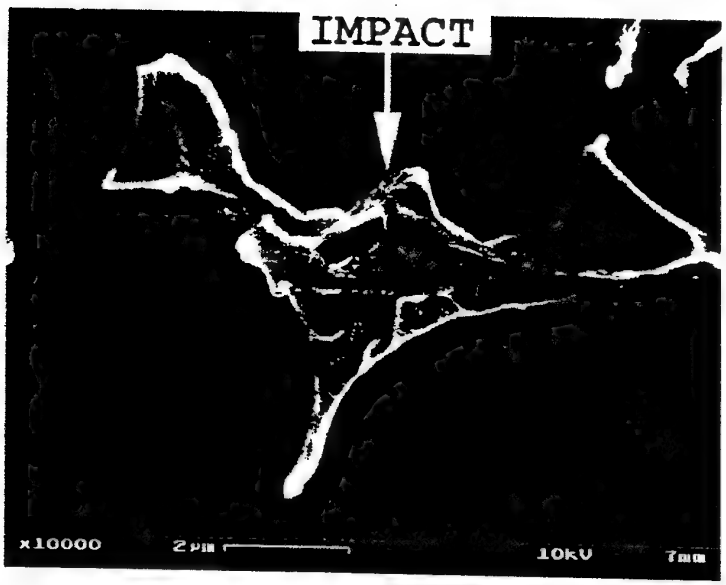

Fig. 9

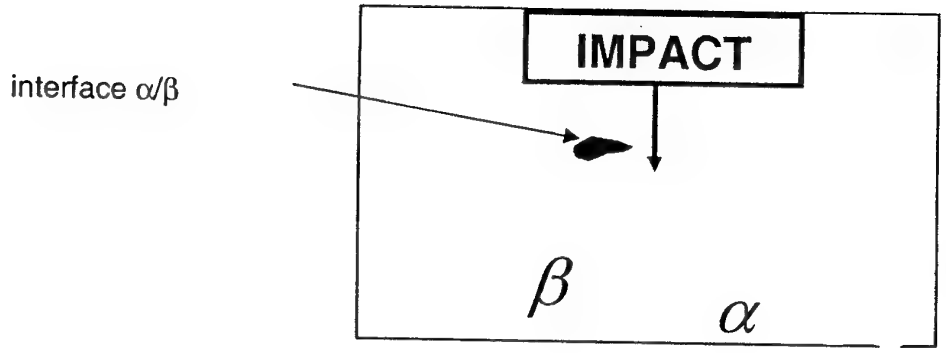

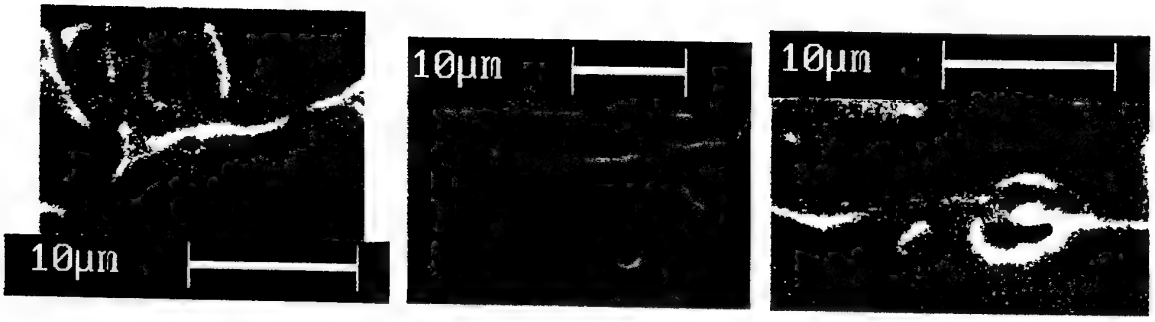

Fig. 10

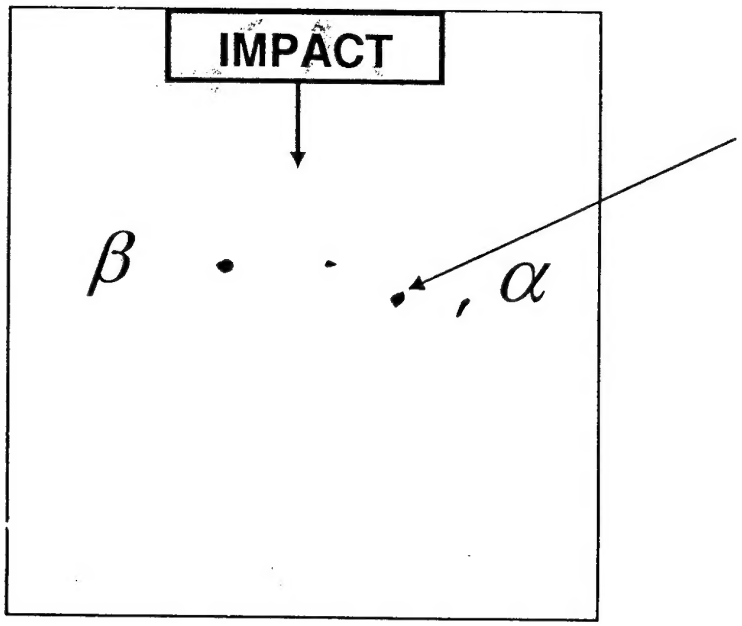

phases β

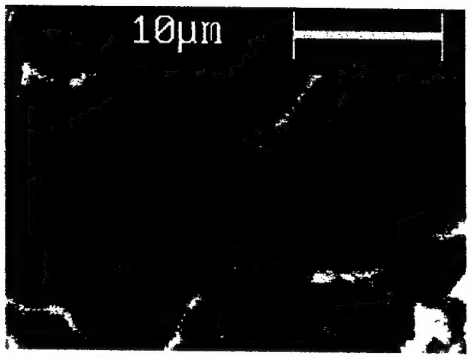

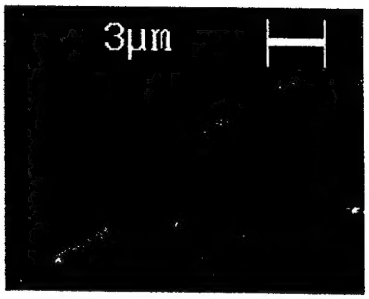

Fig. 11

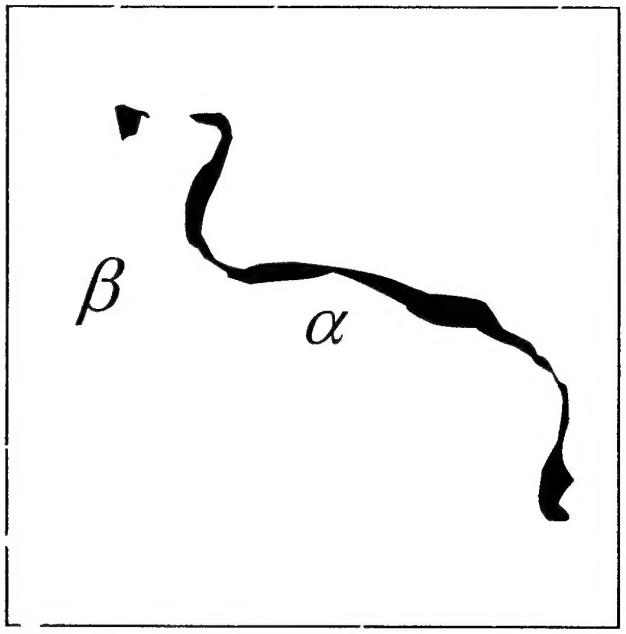

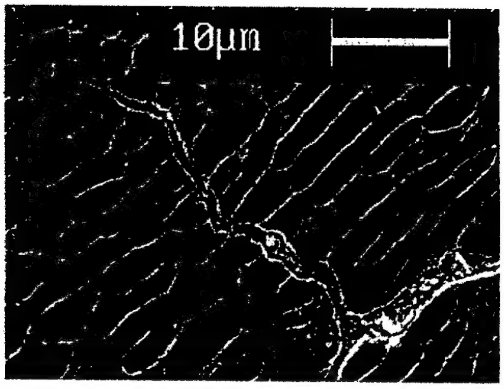

Fig. 12

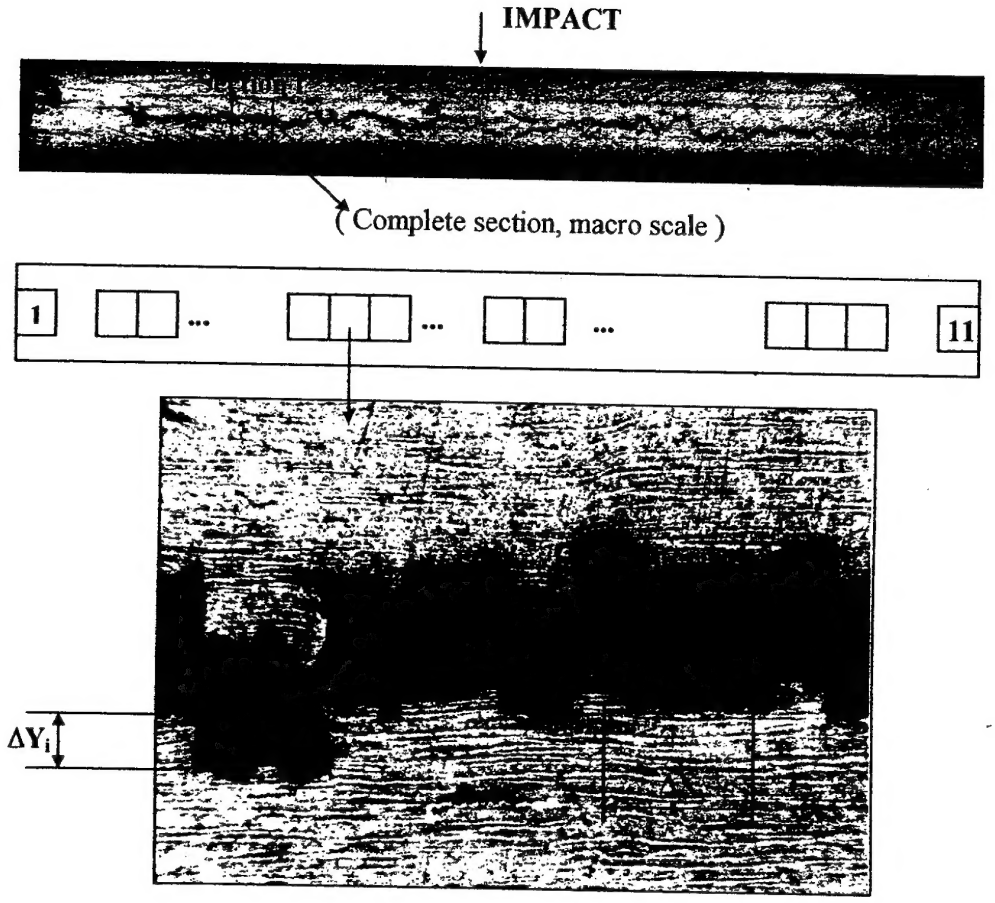

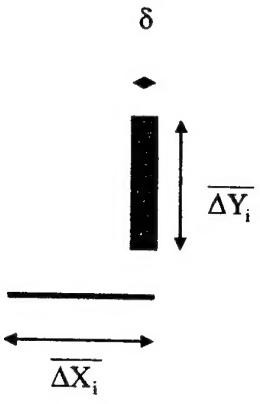

Elementary cell

Fig. 13

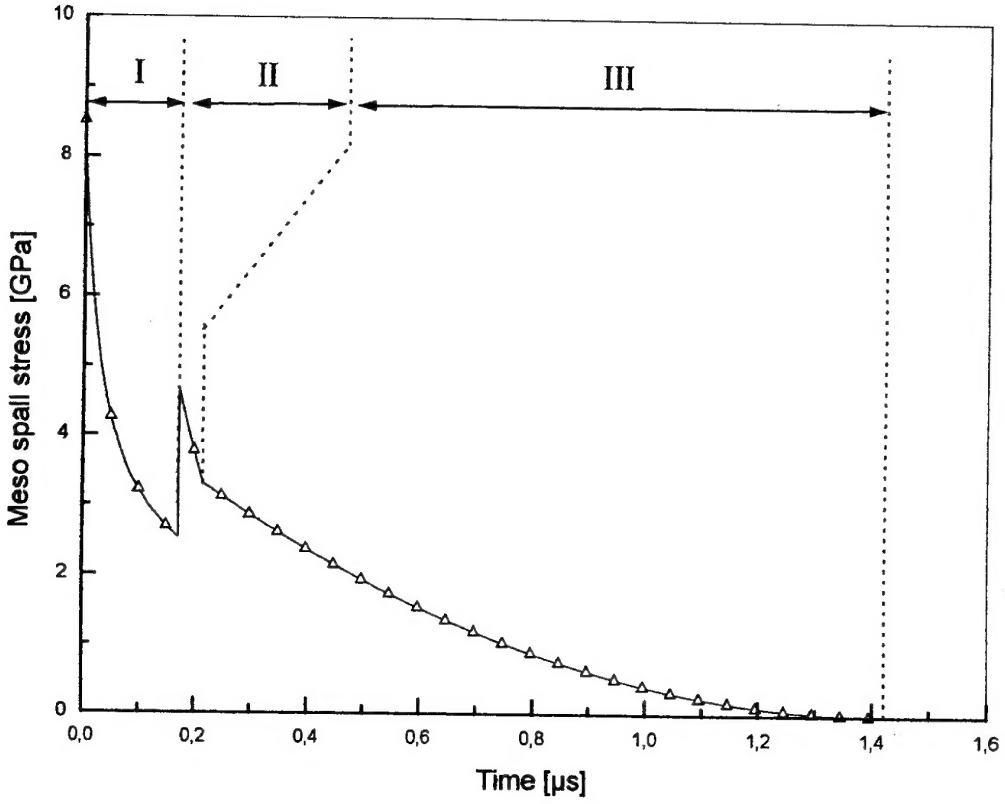
10
8
6
4
2
0
I
II
III
Meso spall stress [GPa]
0,0
0,2
0,4
0,6
0,8
1,0
1,2
1,4
1,6
Time [μs]

Fig. 14